Master thesis.

Endcap ITk Strips module thermal cycle qualification process for Lund University

Author
Eduardo Torres Reoyo
Supervisor
Hannah Herde
Co-Supervisor
Erik Wallin

LUND
UNIVERSITY

May 2024

Abstract

The High Luminosity-Large Hadron Collider (HL-LHC) will reach an approximate pile-up of 200 collisions per bunch crossing, ten times more than the current Large Hadron Collider. Beginning operation at the end of the decade, it will accumulate 3000 fb^{-1}, increasing the chances of observing new processes and allowing measurement of rare processes with higher precision. Moreover, the pile-up increase means more particle production, causing higher radiation damage and detector occupancy conditions. Therefore, the current tracking system in the ATLAS detector will be replaced by the new Inner Tracker system (ITk). ITk is based on silicon detectors, composed of individual sensors and readout electronics called modules. This project concerns testing the module's electrical response to repeated thermal cycling. To perform the tests, a controllable environmental chamber is under construction, The Cold Box.

Popular science

At the end of the 19th century, the only elementary particle known was the electron. However, this changed during the 20th century with the development of accelerator physics and the colliders. By the end of 20th century, all the fundamental particles predicted by the Standard Model were discovered except for the Higgs Boson. To discover the Higgs Boson, it was needed to build the Large Hadron Collider and wait until 2012, when the discovery was announced.

One could think that with the discovery of the Higgs Boson the puzzle was resolved. However, this is far from reality as there are still fundamental questions to answer, such as the nature of dark matter. There are also hints of new physics beyond the Standard Model in the data analyzed from LHC.

To continue this journey, the LHC will be upgraded into the High Luminosity LHC (HL-LHC). Starting operation by the end of the decade, this new upgrade will increase the number of collisions produced, allowing the production and detection of rare processes and even of new processes not detected yet. To detect these processes, it is also necessary to improve the detectors at LHC to keep up with the number of collisions.

One of these detectors is the new Inner Tracker (ITk) at the ATLAS experiment. This detector aims to track the path of the charged particles produced in the collisions. More collisions mean more particle production and more radiation damage suffered by the detectors. Therefore, our detector has to be faster but also deal with the increase in radiation. ITk will be able to deal with these conditions thanks to the silicon detectors that comprise the detector.

The silicon detectors that form ITk need to undergo a quality control process before installing them in the detector structure. Lund University is chosen as a testing site for thermal cycling the process. This process consists of warming up and cooling down the silicon detectors while they are electrically tested. To perform this test, the ITk collaboration has designed an environmental chamber, the so-called Cold Box. My master's thesis consists of preparing the Cold Box received at Lund University to fulfill the requirements established by the ITK collaboration.

Acknowledgements

I would like to express my deepest gratitude to the ITk Lund team, especially to Hannah, Erik, and Lennart. Each of you has helped me in different ways during the course of this thesis. Thank you for welcoming me into your little community.

To my friends, no matter if they are in Lund, Spain, or Belgium, thanks for the support and all the love.

Para mi familia, mi madre Tere, mi padre Antonio y mi hermana Alba, gracias por apoyarme en mis decisions y alimentar mi curiosidad desde niño. Y por supuesto gracias a mis abuelas, Luisa y Lola, sin todo vuestro esfuerzo y constancia no estaría aquí. Y por último a mis abuelos, Tino Y Antonio, que aunque no estén conmigo me inculcaron la pasión por construir cosas.

Index.

Chapter 1

Prefix: from atoms to quarks

The nature of matter has always been a subject of study. What is the matter made of? The first philosophers already wondered this around 3000 years ago. Mochus of Sidon was the first proto-philosopher to write about this [1]. However, it was not until the V-VII century B.C. that the concept of the atom was introduced [2]. In ancient Indian culture, the atom was introduced as *Anu* [3]. However, in ancient Greek civilization, the philosophers used *átomo*, which means uncountable or indivisible, the word used in our era. The concept introduced by this group of Greek philosophers known as the *atomists* school, established a Universe only composed of atoms and a vacuum. However, this idea was lost in occidental culture for many centuries. Modern scientists in the XVIII century rescued it when they had the resources and the freedom to approach the question scientifically. Different famous thinkers wondered about the concept of the atom, but it was John. F Dalton who proposed the first atomic model at the beginning of the XIX century [4], establishing the atom as the fundamental block of nature. Since then, atomic theory gained popularity and many other scientists started researching the atom. Some of the most famous theories are Thomson's plum pudding model, Rutherford's model, Niels Bohr's model, and the atomic orbital model [4]. The latter is currently in use.

Between Dalton's model and the atomic orbital model, 120 years passed. During those years, the electron and the proton were discovered, showing that the atom is not the fundamental block of the Universe. These discoveries opened new questions, and physicists came back to wonder about the fundamental structure of matter. In the 1950s, prototypes of particle accelerators appeared, opening new research topics and giving access to higher energies, eventually leading to the discovery of new particles. Some of these particles seemingly defied the Pauli exclusion principle. In the 60s, Murray Gell-Mann and George Zweig proposed the idea that these "impossible particles" were not elementary particles but were composed of other particles called quarks [5]. After some controversy, this idea was later verified at the Stanford Linear Accelerator Center (SLAC) [6].

Fifty years after this discovery, we know that the Universe's fundamental structure is more complicated than Greek philosophers first thought. Nowadays, we know that the building blocks of matter are the quarks and the leptons. The Standard Model describes the particles and their interactions via three out of four fundamental forces (Electromagnetic, weak, and strong forces; with gravity excluded). Thanks to this model, in only 200 years, scientists have passed from not fully understanding the atom to being able to describe matter's structure and its properties with outstanding precision. Since the development of the Standard Model in the 70s, several experiments have confirmed its predictions. Eventually, all the particles predicted by the Standard Model were discovered,

the Higgs Boson (2012) being the last [7]. However, there are still some open questions and problems that the Standard Model can not answer, such as the origin of neutrino masses or the nature of dark matter. Multiple particle physics experiments have been built or are under construction to answer these questions.

The introduction of colliders combined with the development of detector technology, established a keystone in particle physics history. Enabling access to higher and higher energies, particle accelerators are one of the favorite tools for particle physicists to study the Universe's nature. The largest collider currently operating is the Large Hadron Collider (LHC) [8]. Its construction was approved in 1984 and had the first collisions in 2009, providing humankind with the highest energy collisions ever achieved [9].

The LHC will be upgraded into the High Luminosity Large Hadron Collider (HL-LHC) by decade's end [10]. The main purpose of the upgrade is to increase the number of collisions produced. More collisions imply more events generated, leading to more likelihood of producing rare events or even new physics processes. The upgrade cost is the higher radiation damage and higher occupancy levels in the detectors. To resolve these challenges, there is an upgrade plan for the detectors at LHC. Among all of the upgrades, this thesis focuses on the new Inner Tracker (ITk), which will be installed at the beginning of 2028 as the innermost part of the ATLAS experiment. This thesis describes the work done so that Lund University becomes a thermal cycling site for ITk. To achieve this, it is necessary to commission the Cold Box, an environmental chamber designed to perform electrical tests on the silicon detectors in ITk. The detectors require precise and sensitive control of the environmental conditions, mainly temperature, humidity, and light. The Cold Box has been designed to control and monitor these variables during electrical testing and ensure the tests are carried out under safe conditions for the modules and the people operating the Cold Box.

Chapter 2

Framework

2.1 LHC

The LHC is the largest collider built. It has produced the most energetic collisions ever achieved, providing a center of mass energy of 13.6 TeV in Run 3 [11]. The LHC is located on the border of France and Switzerland. It is one of the facilities built at CERN [12]. The LHC is built in a 27.6 km tunnel, originally constructed for the Large Electron Positron Collider (LEP) [13], the predecessor of the LHC. The LHC's goals include exploring the Standard Model in the TeV region, searching for the Higgs Boson, and investigating open questions such as the nature of dark matter.

The LHC is composed of two high-energy beams that collide at four different points along the ring. To reach TeV-range energies, the particles go through different accelerators at CERN that boost their energy. Once the protons reach the maximum energy possible at one of the accelerators, the particles are dumped onto the next one in the chain. Fig.2.1 shows the different facilities that participate in this process. In addition, it shows the experiments set at the collision points at LHC: ALICE, ATLAS, CMS, and LHCb. Every experiment has a different design, focusing on carrying out different searches and measurements. Section 2.4 contains a more detailed description of ATLAS.

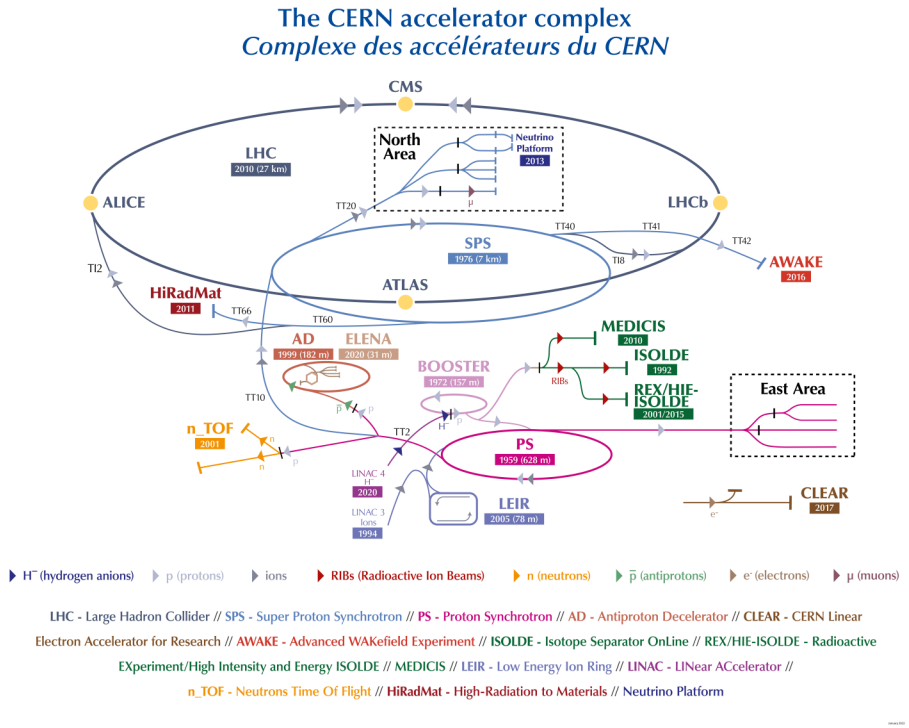

Figure 2.1. CERN accelerators complex and experiments [14].

The particles inside the beam are accelerated to follow the ring geometry thanks to the high-intensity magnetic field generated by superconductive magnets [15]. One of the major challenges introduced by using the LEP tunnel was that the particles used at LEP had opposite charges, while in LHC the particles have the same charge. Hence, in LEP only one magnet was needed to bend the particles in opposite directions. However, LHC needs two magnets occupying the space of one LEP magnet. In Fig.2.2 we can see the two-in-one magnet configuration, the solution proposed to bend the particles in opposite directions in the same ring.

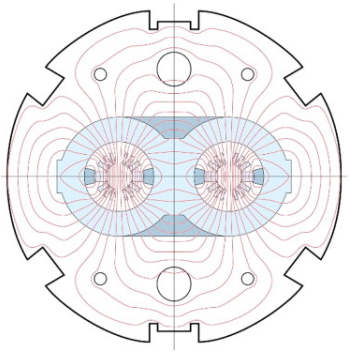

Figure 2.2. Transversal cut of the twin-aperture configuration [15].

The LHC started the commissioning process in 2008, but after an incident, the first physics collisions did not happen until 2010. The collisions were recorded as a center of mass energy of 7 TeV, becoming the most powerful collider in the world [16]. Since then, the LHC has gone through periods of operation, called Runs, and upgrade periods, called Long Shutdowns (LS). After LS2, the LHC increased the center of mass energy up to 13.6 TeV, the operating energy for Run 3 [11]. In addition, instantaneous luminosity increased

over the years. In 2010, the instantaneous luminosity was $\mathcal{L} = 2 \times 10^{32} cm^{-2} s^{-1}$ [16] and for Run 3 the luminosity is $\mathcal{L} = 10^{34} cm^{-2} s^{-1}$ [11]. LS3 is planned between 2026 and 2028. Major upgrades will be performed at LHC, increasing the instantaneous luminosity up to a nominal value of $\mathcal{L} = 5 \times 10^{34} cm^{-2} s^{-1}$ and a final luminosity of $\mathcal{L} = 7.5 \times 10^{34} cm^{-2} s^{-1}$ [17]. This upgrade is known as the High Luminosity upgrade and from that moment on the LHC will be known as the High-Luminosity Large Hadron Collider (HL-LHC).

2.2 HL-LHC

How does the performance of the collider change with the instantaneous luminosity increase? How will this upgrade affect the detectors in the different experiments?

Luminosity is one of the most important parameters of an accelerator. We can distinguish two different luminosities, integrated luminosity and instantaneous luminosity. The former provides a measurement of, in total, how many collisions have been produced over a period of time. Whereas the instantaneous luminosity describes the number of collisions per unit of time [18]. In the following discussion, I will refer to instantaneous luminosity whenever I mention luminosity.

Mathematically, the luminosity of a collider can be expressed in the following way:

$$\mathcal{L} = \frac{N_A N_B n_b f_{rev}}{A}, \tag{2.1}$$

where N_A and N_B are the numbers of particles in a bunch per circulating beam, n_b is the number of bunches in the machine, f_{rev} is the revolution frequency of the collider and A is the effective beam overlap cross-section.

Knowing what the luminosity is, we can calculate how many collisions are produced at LHC and HL-LHC during an hour. To do this, we need to use the following equation:

$$N_{bx/hour} = \frac{\mathcal{L}\sigma_{inel}}{n_b f_{rev}} \cdot \frac{1 \text{ collision}}{25\ ns} \frac{3.6 \cdot 10^{12}\ ns}{1 \text{ hour}}, \tag{2.2}$$

where σ_{inel} is the cross-section for p-p inelastic collisions, this value is 80 μb^{-1} for LHC [8]. Nominal values for these variables are shown in Table 2.2.

Collider	$\mathcal{L}$ $(cm^{-2}s^{-1})$	n_b	f_{rev} (kHz)	$N_{bx/hour}$
LHC	22.6×10^{33}	2400	11.245	$9.65 \cdot 10^7$
Nominal HL-LHC	5×10^{34}	2808	11.245	$1.82 \cdot 10^8$
Maximum HL-LHC	7.5×10^{34}	2808	11.245	$2.74 \cdot 10^8$

Table 2.1: Comparison of the number of collisions per bunch crossing between LHC and HL-LHC

We can also calculate the number of Higgs bosons produced per hour. The number of Higgs produced per hour can be calculated by multiplying the total number of collisions per hour by the rate of the Higgs production, calculated as $\frac{\sigma_H}{\sigma_{pp \longrightarrow XX}}$. The Higgs production cross-section is 58.2 pb^{-1} at 13.6 Tev [19] .The results of this calculation are shown in Table 2.2. HL-LHC will produce up to three times more Higgs per hour than the LHC. Increasing the number of Higgs produced will impact directly the data analysis performance.

Collider	N_H
LHC	70
Nominal HL-LHC	132
Maximum HL-LHC	200

Table 2.2: Comparison of Higgs production per hour between LHC and HL-LHC.

However, the increased luminosity will produce an extremely challenging environment for the detectors. The pile-up is the number of interactions produced that are not interesting. The pile-up increase will cause higher radiation damage and detector occupancy conditions. Therefore, the experiments at LHC will undergo different upgrading programs.

2.3 History of particle detectors

To detect particles, it is needed to make them interact with matter. The electromagnetic interaction typically rules these interactions. Charge particles ionize the matter, and we can detect the product of these interactions. Over the last 120 years, different detection materials have been used, leading to different detection technologies. The first particle detectors were photographic plates. In 1896, H. Becquerel left a photographic plate together with uranium salt. After some time, the photographic plate became black due to the radiation coming from the uranium. Scintillators were also used for detecting particles. One famous example is the use of a zinc sulfide (ZnS) screen by Rutherford, Geiger, and Marsden. Their gold layer experiment used the ZnS screen to detect incoming particles from the gold layer [20].

The cloud chamber was the first detector that made the interaction visible. Charged particles leave a condensation trail in cloud chambers. This trail is the product of the ionization produced by the particles passing through the supersaturated gas that fills the cloud chamber. C.D. Anderson discovered the positron in 1932 thanks to the use of a cloud chamber [20].

In 1950, bubble chambers were developed as a new large-volume detector. The principle behind the bubble chamber is similar to the one used in cloud chambers, but bubble chambers are filled with a superheated liquid. The particles passing through the bubble chamber create bubbles that were photographed. The bubble chamber was key in the confirmation of the quark model thanks to the discovery of σ^- baryon [20].

Until the 1960s, all particle tracks were captured with optical photography. The first detector type using readout electronics was the MultiWire Proportional chamber (MWPC). The MWPC is an array of counter tubes connected to the readout electronics. This technology was further developed into so-called drift chambers. Drift chambers are filled with a gas that is ionized when a charged particle passes. However, this type of detector does not offer good performance in an extremely high-radiation environment like the closest region to the beamline at LHC. For these environments, semiconductor detectors were adopted. In particle physics, this type of detector appeared in the 1980s, but nuclear physics has used them since the 1960s. Semiconductor detectors offer accurate spatial resolution thanks to micro-structuring. Combined with the development of microelectronics, semiconductor detectors became affordable, leading to their use in large-volume tracking detectors as in the LHC experiments [20].

2.3.1 Semiconductor based detectors

The detection idea in the semiconductor detector is similar to the one explained for previous detectors. Charged particles interact with the semiconductor, ionizing the material and producing a signal.

However, natural silicon is not a good conductor. To make it suitable for detectors, the silicon has to undergo *doping*. This process consists of adding impurities to the material. By adding these atoms, silicon's conduction properties can be tuned. The impurities can be classified into two different groups: donors and acceptors [20].

- The donors are atoms that produce an excess of electrons. Materials doped with donors are known as n-type semiconductors.
- If the impurity leads to excess holes, it is known as an acceptor. Materials doped with acceptors are known as p-type semiconductors.

Semiconductor detectors combine these two materials, creating a p-n junction. The performance of the semiconductor detector is highly related to this junction. To understand the behavior of the p-n junction, we need to look at the energy levels of each material and what happens in the junction. The p-type semiconductor is characterized by having the valance band energy close to the Fermi energy. While in n-type semiconductors, the conductive band is close to the Fermi energy. When these two materials create a junction, the charge carriers from each semiconductor diffuse toward the other material. At the boundary, both charge carriers recombine, leading to an area with no charge carriers, the so-called depletion zone, see Fig.2.3 [20].

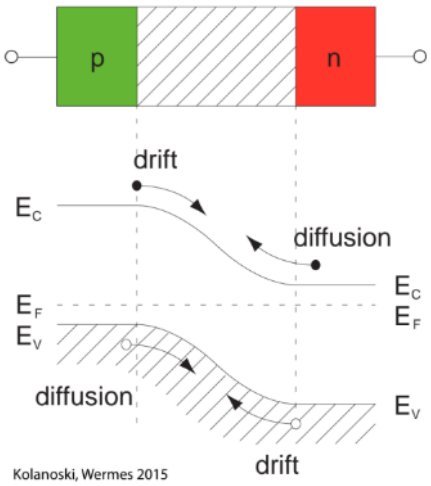

Figure 2.3. Scheme of a pn junction [20].

The depletion zone can be tuned by applying a voltage. If the applied voltage is positive on the n-type side and negative on the p-type side, the depletion region becomes wider. This voltage is known as reverse bias. In the opposite case, the depletion region becomes thinner. The semiconductor detectors operate in reverse bias as the depletion zone is the detecting region. Therefore, the larger this region is, the more likely it is to detect an incident-charged particle. When a particle hits the detector, it creates electron-hole pairs. The pairs drift into the electric field, creating a signal. This is possible because the depleted region decreases the chances of the e-h pairs recombining [20].

In the particular case of ITk Strips, the strip detectors were developed using a technology called n^+-in-p-type [21]. This type of semiconductor technology performs better against radiation conditions than the current tracker at ATLAS. This is a key property of ITk due to the harsh radiation conditions that HL-LHC will create.

The n^+-in-p-type consists of a p-bulk with highly doped n-type implants. The strips are isolated from each other by p-stop and p-spray implants, see Fig.2.4. This layout offers various advantages compared to other combinations of p-n materials. The key aspect is that the amount of signal produced after irradiation is larger. The radiation damage induced by irradiation is acceptor states [22]. Moreover, the signals are generated by collecting electrons. With higher drift velocity and less likelihood of charge-trapping electrons produce a better signal. Lastly, the production cost is up to 50 % smaller compared to the n^+-in-n-type which is even more rad-hard.

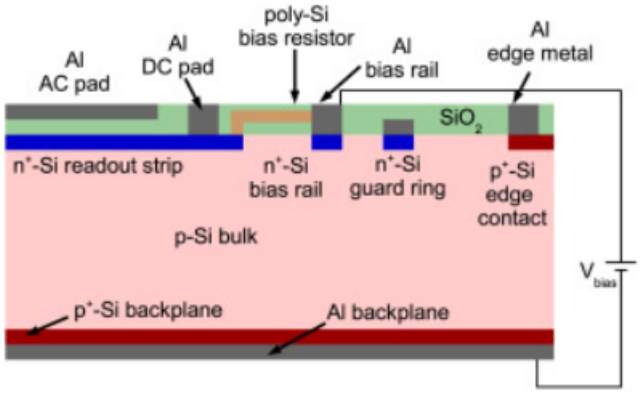

Figure 2.4. n^+-in-p-type strip technology [21].

Another important requirement for the modules is to deal with the high-occupancy conditions created by HL-LHC. The occupancy is defined as the number of detection elements that register an interaction divided by the detector's total detection elements. This is also known as how busy the detector is. If one detector element is busy within the time another particle hits that element, the second particle is missed. The ITk is designed to have a higher detector granularity to reduce occupancy.

2.4 ATLAS

The ATLAS experiment is one of the four major experiments based at the LHC. With its cylindrical shape of 46 m long and 25 m in diameter, it is the largest volume detector ever constructed for a particle collider [23]. Along with CMS, ATLAS is one of the two general-purpose experiments at the LHC. It performs research in a wide range of physics, such as Higgs and top quark studies and dark matter searches.

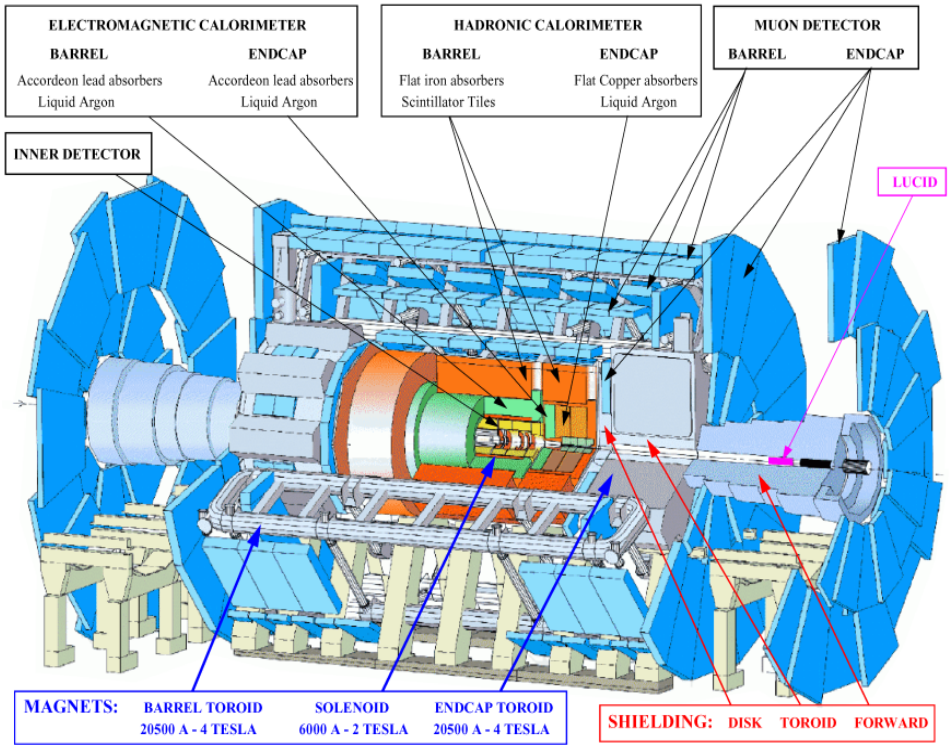

Figure 2.5. Scheme of the ATLAS experiment [24]

In Fig.2.5, the parts of ATLAS are shown. The experiment is composed of six different subsystems, each of them with a specific task. The innermost detector is the Inner Detector (ID). The tracking detectors is composed of different subsystems: the Pixel Detector, the Semi-Conductor tracker (SCT), and the Transition Radiation Tracker (TRT). The goal of tracking detectors is to reconstruct the trajectory followed by charged particles inside the detector and perform vertex reconstruction. In addition, tracking detectors can provide momentum measurements by adding a magnetic field that deflects the particles. The ID is in a 2 T solenoidal field. Tracker systems are designed with different layers, as shown in Fig.2.6, to measure how the particles move through the detector. A charged particle will leave a hit in each layer, indicating its trajectory. It is important to remark that neutral particles, like photons, will not create a signal in this type of detector. The current ATLAS tracker has a length of 6.2 m and extends to 105 cm from the beam line. It covers a pseudorapidity range of $|\eta| < 2.5$. It has a total of 92 million pixels and six million strips.

Calorimeters surround the ID. The purpose of the calorimeters is to measure the energy deposition of the incoming particles. From the ATLAS center to the outer parts, one can find the electromagnetic calorimeter and the hadronic calorimeter. The electromagnetic calorimeter aims to measure the energy deposition produced by electromagnetic interaction. The hadronic calorimeter focuses on measuring the energy deposition produced by the strong interaction. Lastly, the outer part of the experiment is the Muon Spectrometer in a toroidal magnet field. The purpose of this detector is to measure the muons' momenta.

2.5 Inner Tracker System

As mentioned in Chapter 1, this thesis focuses on the new Inner Tracker system (ITk), which will replace the current ATLAS ID by 2028. With a length of 6 m and a diameter of 2 m, ITk comprises two types of detector technology: pixels-based detectors, used in the innermost layers where higher occupancy conditions require more resolution, and strip modules for the outer layers. ITk is divided into substructures: the smallest ones are the modules, which are placed in a local support structure, and installed into global supports [22].

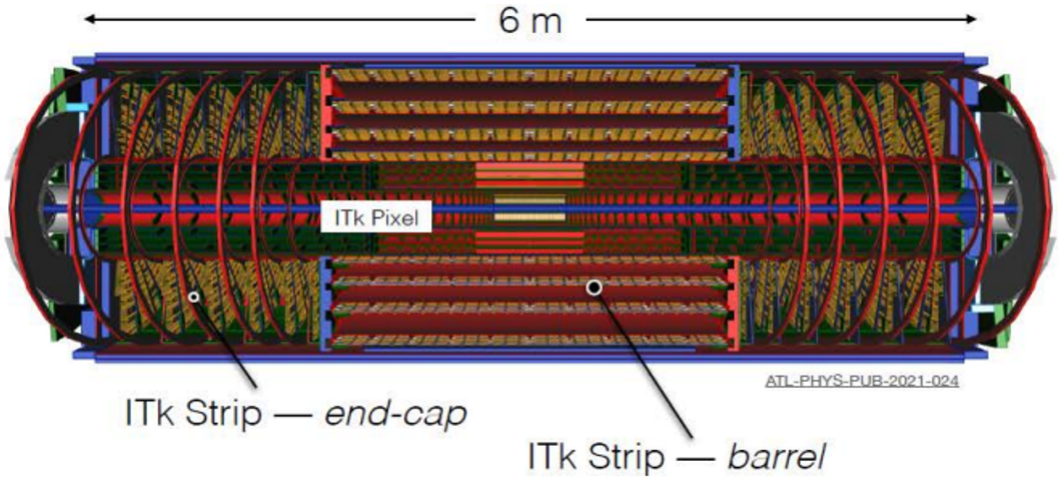

Figure 2.6. Scheme of ITk [25].

ITk has two main subsystems based on detector technologies: ITk Pixels, and ITk Strips. At the same time, each subsystem is divided into Barrel and Endcap. In Fig.2.7, a map of active material in ITk is shown. The work done at Lund University is related to strip modules for the Endcap part, hence this thesis will focus on describing the ITk Strip System.

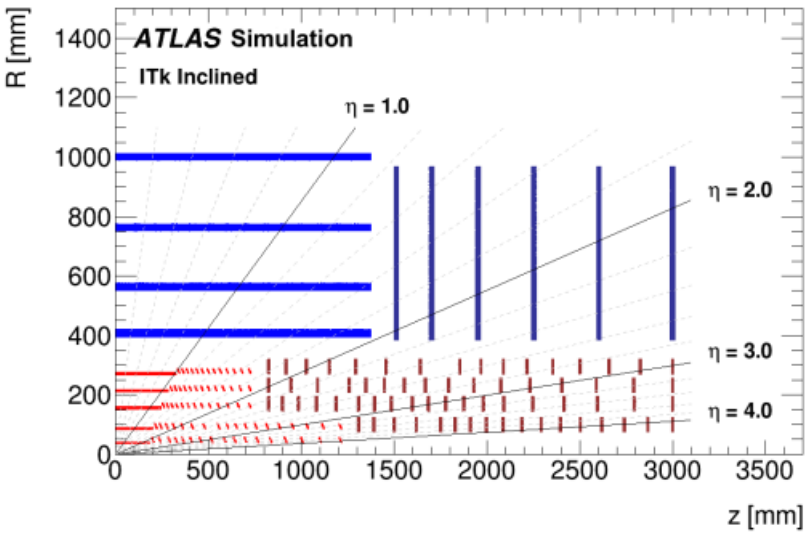

Figure 2.7. Layout of ITk [25].

ITk offers a pseudorapidity range $|\eta| < 4.0$. It has 60 million strip channels and 1.4 billion pixels. Comparing these characteristics with the current ATLAS current tracker system, the pseudorapidity range increases for covering the forward region. The number of detector components also increases, ten times more strip channels and 55 times more pixels. It is expected that the occupancy conditions are kept under 1%.

2.6 ITk Strip system

In Fig.2.7 the ITk Strips layout is shown in blue. The barrel region comprises four layers of detectors mounted on staves, the local support structure where the strip modules are placed. The endcap comprises six disk-shaped layers composed of petals, the local support structure designed for the endcap. Both local support structures provide a structure to place the modules, carry power to the modules, provide cooling, and collect the data measured in the modules. The core structure is made of carbon fiber with space for the cooling pipes. The outer layer is made of co-cured carbon fiber with bus tape.

2.6.1 ITk Strip modules

The modules are the smallest units of the ITk Strip detector. The modules are made of a silicon sensor and electronics, as shown in Fig.2.8. The electronics handle powering, control clock and trigger signals, and data readout. Building a module consists of gluing the electronics onto the silicon using epoxy glue [22]. Then, wire-bonding establishes all the electrical connections.

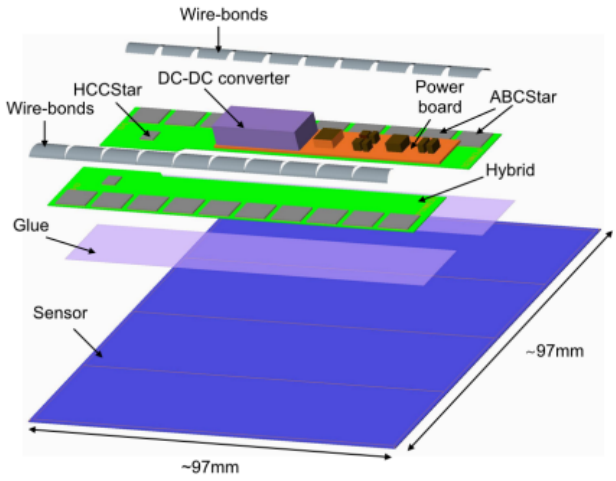

Figure 2.8. Composition of an LS module, where the different parts of the module can be observed [22].

Modules have between one and four hybrids. The hybrid design is adapted to different modules geometries however, the functionality is the same in all cases. The hybrid is a Printed Circuit Board (PCB) designed to provide power and grounding to the Application-Specific Integrated Circuits (ASICs) and to establish communication with the electronics in the local supports' End-of-Structure (EoS) PCB. In the case of ASICs, the number of components changes depending on the module type. Two different ASICs are part of the hybrid, the ATLAS Binary Counter (ABC) and the Hybrid Controller Chip (HCC). The

HCC interfaces the stave/petal service bus and the front-end ASICs. The HCC receives the signals coming from the different ABCs and packages them with those. Then, it sends the package to the EoS through the bus tape on the local support. In addition, it receives the clock and control signals and sends them to the ABCs. One HCC can control up to 11 ABCs. Each ABC has 256 input/output pins. Each strip has two connections with one ABC, using two different pins. The functionality of the ABCs is to transform the signal generated in the strip into a binary signal. All ABCs channels are connected to the strips through a wire bond with a thickness of half of a human hair, $25\mu m$. All modules have a strip pitch of $74,5\mu m$

Each module has one radiation-resistant power board (PB). The PB is composed of a DC-DC converter, the Autonomous Monitoring and Control Chip (AMAC), the HV multiplexer, and the HV bias filtering circuit. The AMAC monitors different parameters on the modules: voltage, bias current and temperature. Moreover, the AMAC controls the power distributed to the hybrid and provides a clock signal.

In the case of the barrel, two different types of modules can be found. Short-strip modules (SS-modules) and Long-Strip modules (LS-modules) are shown in Fig.2.9a and 2.9b respectively. The footprint of each type of module is the same, but SS-modules have two hybrids while LS-modules only have one. For the SS modules, the strip length is 24.1 mm, while for the LS modules it is 48.2 mm. This direction is defined as the Y direction of the module. The SS modules have higher resolution in the Y direction. The smaller strip length leads SS-modules to deal better with higher occupancy conditions. The hybrids for these modules contain ten ABCs that a single HCC controls. Each ABC reads 128 strips for a total of 1280 strips per LS module.

(a) SS module. **(b)** LS module.

Figure 2.9. a)Photo of an SS module taken during the March 2024 testbeam campaign. b) Photo of an LS module taken at Lund University.

The complex geometry of the endcap, designed to maximize coverage, is achieved with different endcap modules geometries. There are six different flavors of the endcap modules: R0, R1, R2, R3, R4, R5. In Fig.2.10, the endcap modules are shown. The design of the module adapts to the endcap geometry. The modules have a wedge shape with curved edges and radial strips. Moreover, different flavors have different strip lengths. As in the barrel case, modules placed closer to the beam must deal with higher occupancy conditions. Therefore, these flavors have shorter strips.

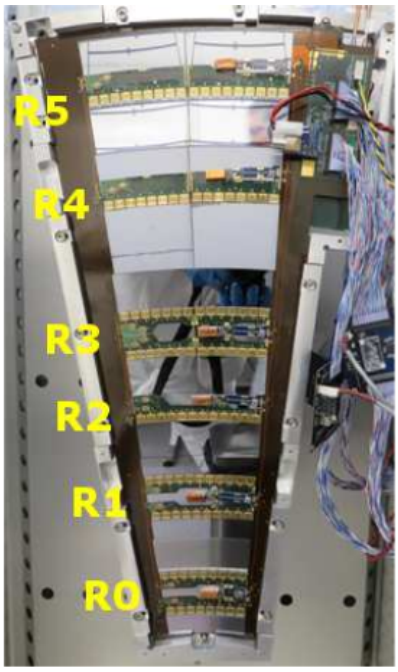

Figure 2.10. Different endcap modules loaded onto a petal [26].

2.6.2 Barrel

The Barrel is the central part of ITk Strips. It comprises four layers of modules, divided into two layers of SS modules and two layers of LS modules. The SS modules are placed closer to the beam. The closer to the beam the layer is, the more resolution is required. Each layer consists of an array of staves. The strips are placed parallel to the beam axis. In total, there are 392 staves in ITk [22].

On each side of the stave, 14 modules are glued for 28 modules total. Moreover, the modules are placed on the staves with a rotational angle of 26 mrad with respect to the beam axis, allowing a total stereo angle of 52 mrad between the staves' sides [22]. The idea behind this rotation is to provide a second particle measurement and increase the surface covered by the modules. In Fig.2.11 a stave is shown.

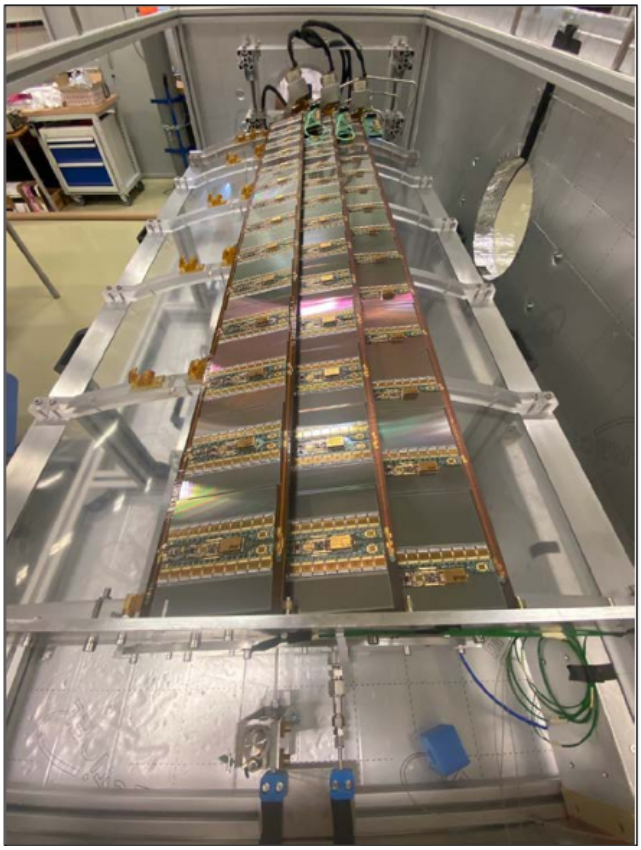

Figure 2.11. Three staves prepared for testing. [27].

2.6.3 Endcap

ITk strips has two endcaps, one on each side of the barrel. The endcap comprises six disk-shaped layers as shown in Fig.2.12. At the same time, the disk is divided into rings concerning what type of module is placed on it. The module type chosen for each ring keeps occupancy below 1%. Therefore, the R0 modules, with the shortest strips, are placed in the innermost part of the disk, while the R5 modules, with the longest strips, are placed in the outer part [22].

Each disk is formed by 32 petals and six modules are glued on each side of the petal. The modules are designed in a specific way that produces a total 40 mrad stereo-radial angle with respect to the beam axis, 20 mrad per side.

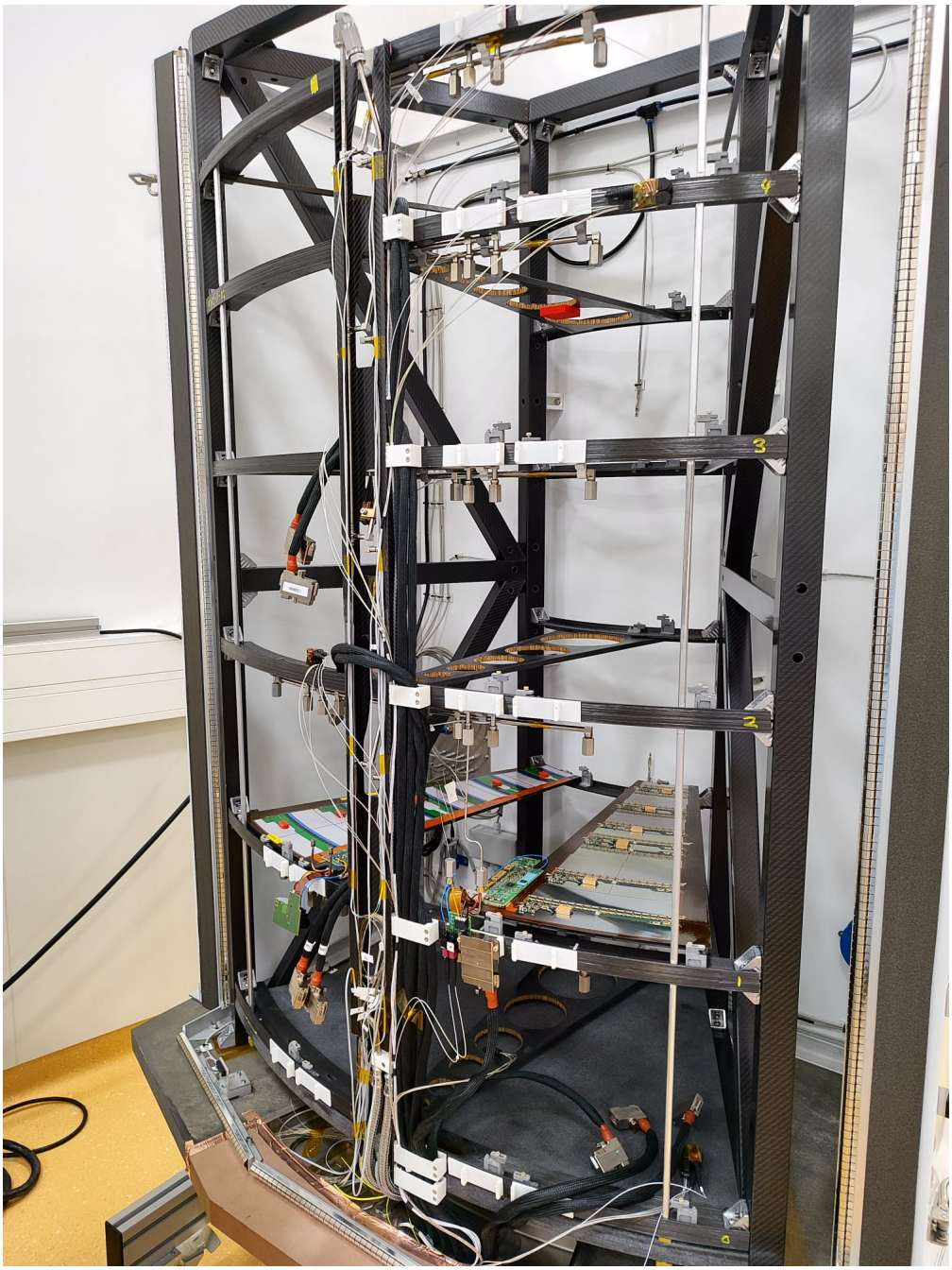

Figure 2.12. Photo taken during the March 2024 testbeam campaign of the Endcap structure with a module loaded.

Chapter 3

The Cold Box

Before starting to test ITk Strips modules regularly, Lund University team must demonstrate we can perform reliable-quality control tests, particularly thermal cycling on the endcap strip modules. To perform thermal cycles, the ITk team at DESY, Hamburg, designed the Endcap Cold Box. The sensitivity of the modules requires the installation of the Cold Box in a clean environment. The Cold Box is an environmental chamber that allows the user to control temperature, humidity, and prevent light leaks. The modules are electrically tested on so-called *chucks*, which provide grounding, mechanical support, and temperature control for the modules. Each chuck has a copper bottom and an aluminum top half, see Fig.3.1b. Peltier plates are placed between these materials to regulate chuck temperature. Lastly, the aluminum is covered with a Kapton layer to provide electrical insulation between the chuck and the modules.

This master's thesis focuses on commissioning the Cold Box at Lund University. The commissioning document submitted to the ITk Strip collaboration as part of Lund University's "site qualification process" is included in the annex.

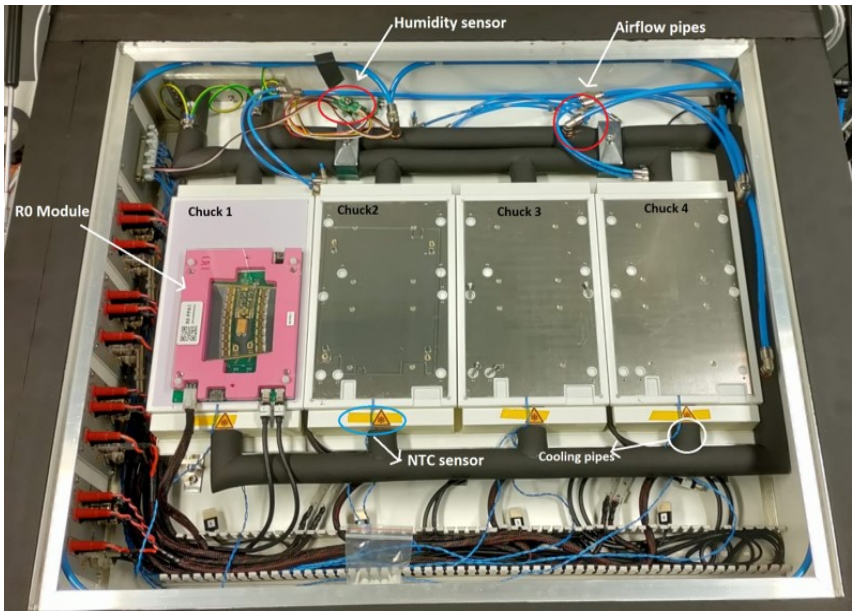

(a) Inside of the Cold Box.

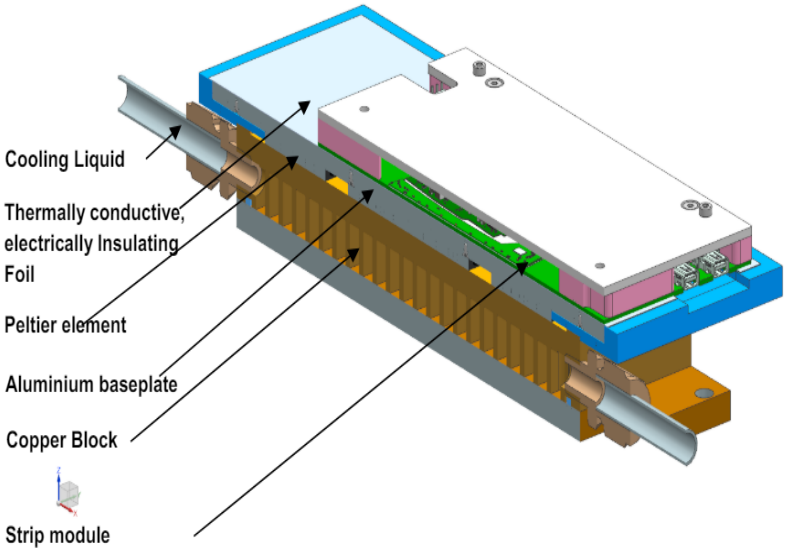

(b) Chuck structure.

Figure 3.1. a)Photo of Lund's Cold Box. The different components of the Cold Box are labeled. b) Internal structure of a chuck [28].

In Fig.3.1a, the inside of the Cold Box is shown. At Lund University, we have an Endcap Coldbox. This Cold Box flavor is designed to test endcap strip modules. We can test up to four modules simultaneously, one on each chuck. The basic idea behind the design is to control and monitor the Cold Box using a Raspberry Pi and to perform the electrical tests using the Data Acquisition (DAQ) computer. The modules need to go through thermal cycling as part of the quality control. The thermal cycling sequence consists of cooling down and heating up the temperature of the modules between $-35°C$ and $20°C$. The process is repeated for a total of ten cycles, followed by two hours of high-voltage stabilization at room temperature. A thermal cycling sequence is shown in Fig.3.2 Section 3.4 describes the thermal cycling sequence in more detail. The lower temperatures of the cycles match the operating conditions of the modules in ITk, $-35°C$.

After thermal cycling, the module is evaluated as pass or fail. If the module passes the test, it is sent to IFIC, DESY, or Freiburg University for incorporation into a petal. Failed modules are removed from the production chain.

Figure 3.2. Thermal cycle sequence defined by the ITk Strip collaboration [28].

3.1 Cooling principle

The temperature must be stable while the module is being tested. Additionally, the temperature gradient can not be larger than $2.5°C/min$ throughout the thermal cycling sequence. The Cold Box has two methods to control the temperature: a coolant fluid with a chiller and Peltier plates. Moreover, the Cold Box has a bypass valve controlling the coolant circuit. When the bypass valve is opened, coolant flows through the Cold Box.

The purpose of the chiller is to decrease the average temperature of the environment in the box. The coolant runs through the copper block, providing a heat sink for the Peltiers. The Peltier plates are in charge of providing the last degrees of the cooling cycle and warming up the Cold Box. The Peltiers also stabilize the temperature.

The Cold Box has three working modes: IDLE, HEAT, and COLD. Depending on the cycling stage, the Cold Box will change between modes. For the IDLE mode, the chiller is set to a target temperature, the bypass valve is opened and there is no current running through the Peltier plates. The IDLE mode is used during the Pre-Cycling Sequence at room temperature. If the Cold Box is set to COLD, there is a current on the Peltiers, the chiller temperature is set to $-30°C$, and the bypass valve opens. This mode is used when the target temperature is $-35°C$. In the case of the HEAT mode, the polarity of the Peltiers is switched and the bypass valve closes. The chiller set temperature is still $-30°C$, even in the HEAT mode. This mode is used during the warm-up parts of the thermal cycling.

During thermal cycling, both methods work together to achieve the desired temperatures. When the Cold Box is cooling, the Peltiers' current runs from positive to negative, generating a positive temperature gradient from the aluminum to the copper. Meanwhile, the coolant running through the copper keeps the copper cold, acting as a heat sink for

the heat generated by the Peltier. If the Cold Box is heating, the chiller is still set at $-30°C$, but the coolant circuit is disconnected by closing the bypass valve. Hence, coolant does not flow through the Cold Box pipes. In addition, the Peltiers' polarity is switched, generating a positive temperature gradient from the copper to the aluminum. Switching the polarity is achieved thanks to a polarity switch connected to the PITk board designed by A. Ekman [29].

3.1.1 Peltiers Plates

The Peltier plate is a thermoelectric device that uses the Seebeck effect and Peltier effect as running principles. The Seebeck effect is produced when a voltage is generated between two conductor or semiconductor materials because of a temperature gradient. The temperature gradient causes electrons to diffuse from one material to the other [30]. The Peltier effect is produced when a voltage difference is established across a junction of two conductor or semiconductor materials. This effect generates the absorption or the emission of heat, creating a temperature change in the junction. The heat flow direction is defined depending on the materials and the current direction, making the Peltier effect reversible [30].

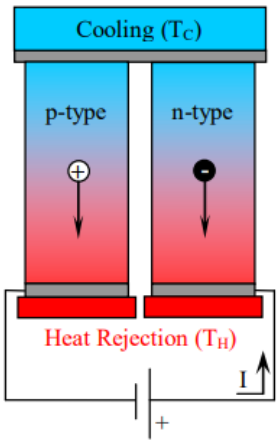

Figure 3.3. Thermoelectric couple created by joining two semiconductors with a metallic strip [30]

The Peltier device structure used in the Cold Box can be seen in Fig.3.3. The Peltier device comprises several of these Peltier blocks. Each block consists of a p-type and n-type semiconductor connected by a metallic strip. Four metal-semiconductor junctions are created per block. A larger temperature difference between the plates is achieved by connecting several of these blocks in series. Heat is absorbed or emitted in the metal-semiconductors junctions as the charge carriers from the semiconductors cross the junctions. There are four possible junctions depending on the current direction: metal/n-type, metal/p-type, n-type/metal, and p-type metal. As current passes through the metal/n-type semiconductor junction, an electron acquires energy (cooling) as it enters the conduction band, see Fig.3.4a. The opposite happens when the current passes across the n-type/metal, see Fig.3.4b. In the p-type/metal junction, heat is absorbed, see Fig.3.4c while in the metal/p-type junction, heat is released, see Fig.3.4d.

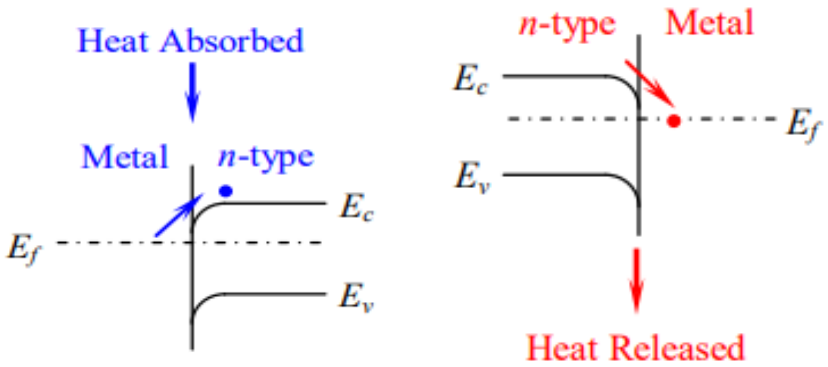

(a) Energy band scheme of metal/n-type junction.

(b) Energy band scheme of n-type/metal junction.

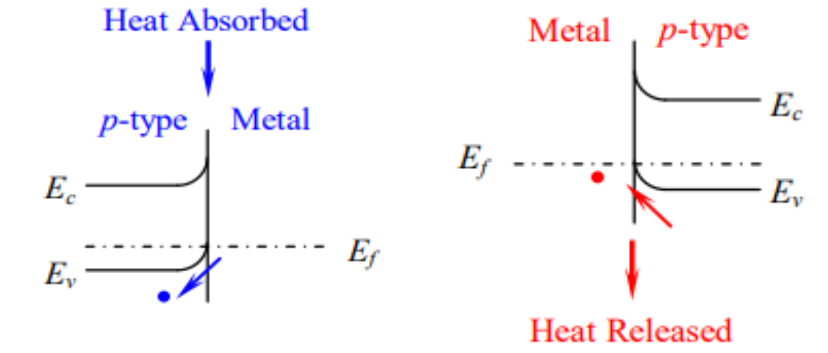

(c) Energy band scheme of p-type/metal junction..

(d) Energy band scheme of metal/p-type junction.

Figure 3.4. Different energy band diagrams for ideal metal-semiconductor junctions for thermocouple blocks [30].

In the Cold Box, each chuck has four Peltier plates. The Peltiers are connected to a polarity switch and the power supplies. The polarity switch allows us to change the Peltier plates between HEAT and COOL modes. The Raspberry Pi controls the current by setting proportional-integral (PI) control parameters: the proportional current (k_p), the integral current (k_i), and the limit current. The PI controller ensures the temperature gradient is always kept under the $2.5°C/min$ requirement. The closer the temperature is to the target temperature, the smaller the change in the current is. The thermal cycles before and after configuring the PI parameters are shown in Fig.3.5.

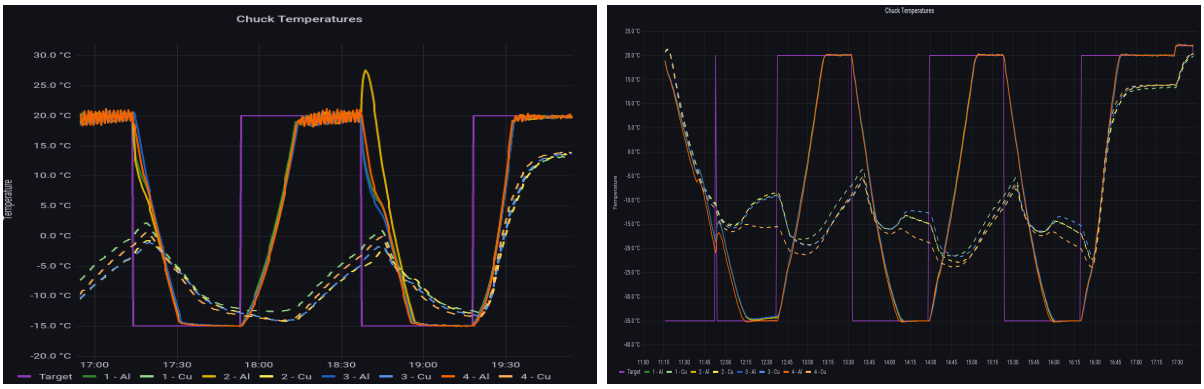

(a) Before configuration.

(b) After configuration

Figure 3.5. Result of the configuration process of the Peltier plates. a) Before configuring the PI parameters, big increases in the chuck temperature are observed when approaching the target temperature. b) After configuring the PI parameters, the chuck temperature approaches smoothly to the target temperature.

The biggest advantage of Peltier plates is that they control temperature precisely, keeping the desired temperature stable. However, Peltier plates are inefficient, subject to the Joule effect. A second cooling source is needed to reach the temperature required for the test.

3.1.2 Chiller

The second source is a chiller with a coolant liquid. The chiller is placed outside of the clean room. It is connected to the Cold Box using vitron pipes. The bypass valve controls when the coolant runs into the Cold Box. The coolant used is a silicone oil called Polydimethyl siloxane. The main requirement for the coolant is to have a freezing point lower than $-35°C$.

By default, the Raspberry Pi sets the chiller temperature during the thermal cycling to $-20°C$, and the Peltier plates start running at $-15°C$. However, in Lund's case, this configuration is not sufficient to reach $-35°C$ when four modules are connected in the Cold Box. Depending on the module's type, it dissipates between 4 and 6 W. This power is not big compared to the Peltier plates' power dissipation (up to 90 W). However, it is enough to prevent reaching $-35°C$ with the default configuration. To simulate a loaded Cold Box and perform a stress test, I installed heat pads on the Cold Box. These tests aimed to find the optimal configuration of the chiller temperature and starting parameters of the Peltier plates. The chiller can dissipate up to 370 W at $-30°C$. Between the Peltier plates and the modules, the power to be dissipated is around 360 W. If the Peltier plates activate too early, the chiller cannot deal with the heat generated and the chucks never reach $-35°C$.

Therefore, the final configuration runs the chiller at $-30°C$ and starts running the Peltier plates at $-25°C$. Using this configuration, the Cold Box can reach $-35°C$ even loaded with four R3 modules, the kind that dissipates the most power. Running the chiller colder will increase the first cool-down of the TC sequence significantly.

3.2 Environmental sensors and control systems.

There are different control systems and environmental sensors installed in the Cold Box to control and monitor the environment. These devices can be divided into two categories. On one hand, environmental sensors such as relative humidity sensors help us to monitor the environment. On the other hand, control systems help us to control the environment, such as the airflow meter or the interlock system.

3.2.1 Environmental sensors

Three environmental variables are controlled by the Cold Box: temperature, relative humidity, and light. Each of them is monitored and corrective actions can be taken if the parameters exit their safety windows.

The temperature is monitored using Negative Temperature Coefficient Thermistors (NTC). NTCs are semiconductor devices where the resistance depends on the temperature. The NTC resistance decreases as the temperature increases according to the following expression:

$$R_{NTC} = \frac{U_x R_x}{U_{ref} - U_x}(\Omega), \tag{3.1}$$

where R_x is the resistance value at $25°C$, U_x is the voltage output from the NTC, and U_{ref} is the voltage of the Raspberry Pi.

To calculate the temperature, the following expression is used:

$$T = \frac{B}{ln(R_{NTC}/R\infty)}(°C), \tag{3.2}$$

where B is a constant from the NTC and $R_\infty = R_x \cdot e^{-B/T_0}$ is the dependency of the resistance with the temperature. Therefore, by measuring the resistance, the temperature can be calculated.

The temperature is monitored in two places on each chuck for a total of eight NTCs in the Cold Box. One NTC is placed on the copper and the other one is placed on the aluminum, see Fig.3.1b. It is assumed that the temperature on the NTC and the chuck is the same as we have ensure good thermal contact. The NTCs are connected to the Raspberry Pi through the PITk-board designed by Alexander Ekman from Lund University [29]. The thermal cycle is defined by the temperature measured on the aluminum chuck, as it is in direct contact with the module. Before installing the NTCs in the Cold Box, it is necessary to calibrate the sensors. The calibration consists of finding the B constant of the NTCs. The calibration was done by Lennart Österman. After calibration, we installed the NTCs in the Cold Box. The last step was to update the B parameter in the software configuration file and check that the values measured were reasonable.

In addition to temperature, relative humidity (RH) is also controlled in the Cold Box. To operate the modules safely in the Cold Box, a low relative humidity environment has to be achieved. Two pipes pump dry air into the box. One distributes the air throughout the Cold Box and the other one provides dry air directly to the modules. The latter is connected to the modules through smaller pipes, see Fig.22 from the appendix. The idea is to have a constant dry airflow over the module while it is under testing.

The RH inside the Cold Box is measured using five sensors: one measures the RH of the Cold Box itself and the other four measure the RH of the air coming out of the modules. It is important to measure RH because the inside of the Cold Box could freeze

during the cold phase of a thermal cycle. This freezing point is known as dewpoint and is calculated from relative humidity and temperatures. The RH sensors are connected to the Raspberry Pi using the IC2 connection. The RH sensors can measure the temperature used to calculate the dewpoint (DP).

The sensors chosen for the Cold Box have shown an offset in the humidity measured that increases with time. According to a study done by Erik Wallin, the humidity sensors had an offset between 1.5-2.5%. To try to reduce the offset, the RH sensors were baked for three days at $80°C$. After the baking process, the offset decreased to 0.25-0.4%. To study offset evolution, the RH is recorded every week.

As mentioned in Section 3.2, the Cold Box also protects the modules from light leaks. The Cold Box has a light-tight lid. The lid is monitored using the interlock system of the Cold Box, explained in more detail in section 3.2.2.

3.2.2 Control sensors

The RH is controlled by the airflow meter and two valves that control the dry air flow entering the Cold Box. One valve controls the dry air pumped to the module, while the other one controls the dry air pump to the Cold Box in general, see Fig.3.6a. The airflow meter is connected to the Raspberry Pi using an Analog Digital Converter (ADC) board. The output signal coming from the airflow is a voltage (analog). Then, the ADC board converts it into a digital signal. However, the airflow meter's raw voltage exceeds the range of the ADC so the airflow meter is in a voltage divider, see Fig.3.6b.

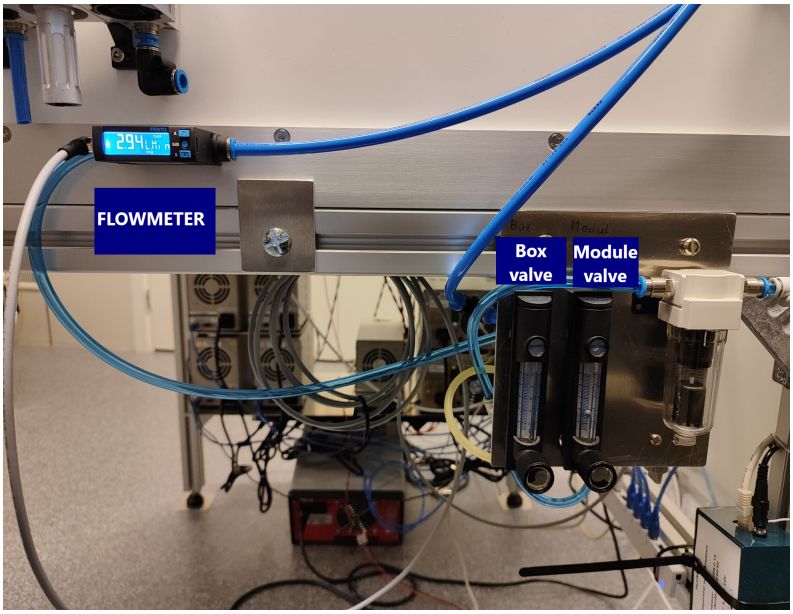

(a) Side of the Cold Box where the air flow system is appreciated.

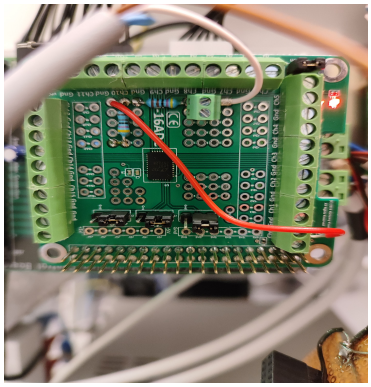

(b) ADC board installed to connect the flowmeter to the Raspberry Pi.

Figure 3.6. Airflow system of the Cold Box. a) The airflow meter syteam of the box is shown. b) the voltage divider soldered in the ADC to connect the flowmeter to the Raspberry Pi.

The Cold Box also has a safety system or interlock. The interlock protects both modules and Cold Box users by shutting down safely the Cold Box in the event of a malfunction. Moreover, a physical interlock in the Cold Box prevents access and is connected to the software-based interlock.

If the temperature of any chuck is higher than $30°C$ and lower than $-45°C$, the interlock system will correct the temperature to safe values.

If the RH is higher than 70%, the interlock system will warm up the box to room temperature. During thermal cycling, the dewpoint has to be lower than $-40°C$. If this condition is broken the interlock system stops the thermal cycle sequence and warms up the box to room temperature.

The last scenario regarding the environmental conditions is opening the Cold Box during a thermal cycle. The interlock system locks the box whenever the temperature of any chuck is lower than $15°C$. If the Cold Box is opened during the thermal cycle sequence, the interlock system stops the the thermal cycle and jumps directly to the final warm-up sequence.

The maximum high voltage (HV) used during a thermal cycle is 550 V, hence, a safety system is necessary to protect the users. The first safety measure is that the Cold Box is grounded, see Fig.18 from the appendix. The second safety measure is that the Cold Box locks whenever the HV is on. If the Cold Box is opened while the HV is on, the interlock system switches off the HV.

The physical interlock is connected to the software interlock with a PCB developed at Lund University, see Fig.3.7. The main design idea behind the PCB is to use a transistor as a switch. The interlock PCB controls the physical interlock in the Cold Box and the interlock system of the HV power supply. We can follow the status of the HV and the lid of the Cold Box using this system. The PCB is connected to the Raspberry Pi via the GPIO connections.

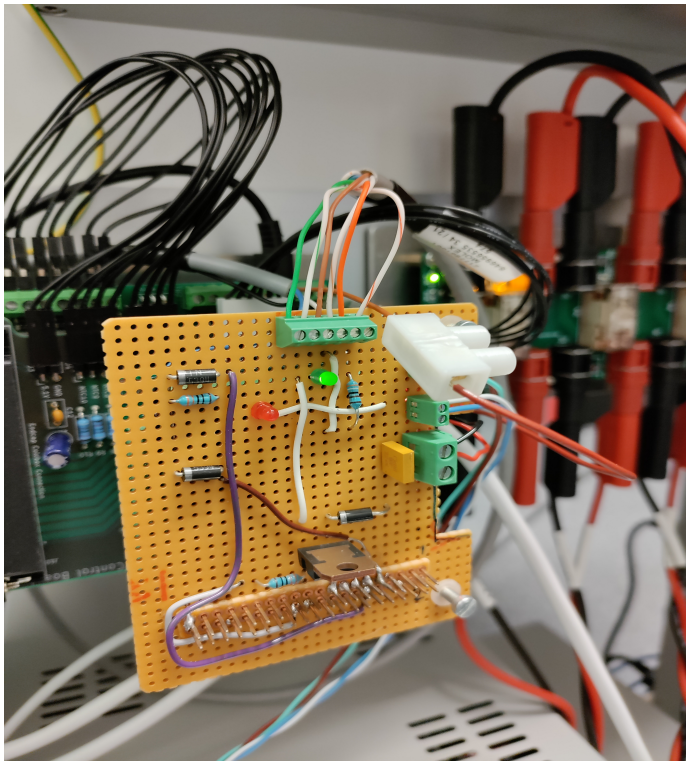

Figure 3.7. Interlock PCB connected to the Rapsberry Pi.

3.3 Software of the Cold Box

Two software systems are implemented in the Cold Box. The Coldjiglib software installed on the Raspberry Pi controls the environmental information and the thermal cycle sequence. ITSDAQ is installed on the DAQ PC, controls the electrical testing of the modules.

3.3.1 Raspberry PI and Coldjiglib

The Raspberry Pi is a single-board computer. It offers the possibility to control different devices thanks to different connections. Moreover, the number of connections can be increased using peripherals like the ADC board or custom PCBs like Lund's interlock PCB. The Coldjiglib environment is installed on the Raspberry Pi.

The Coldjiglib environment was developed specifically for the Cold Box. It is designed to receive information from the different sensors in the Cold Box and store it in a database called INFLUX. Coldjiglib controls the thermal cycling sequence. Coldjiglib also provides a Graphical User Interface (GUI) to control the Cold Box. Using the GUI, the Cold Box user can start an automated thermal cycle or control the Cold Box manually.

To visualize the environmental data coming from the Cold Box, we use Grafana. This program is a visualization software that connects to INFLUX and shows the information in real time. Using Grafana, we can display the environmental parameters of the Cold Box, the Peltier plates, and the module's status, see Fig.8 from the appendix.

3.3.2 Data acquisition software

Two threads of the data acquisition software ITSDAQ are run while testing a module, one for performing electrical tests and one for monitoring the AMAC. ITSDAQ is in charge of communicating with the modules and controls the electrical testing. When a module is connected to the Cold Box, we need to tell ITSDAQ which module type is under testing. Then, we establish communication with the AMAC. After this, we can run any test on the module, manually or through the thermal cycle sequence. Once the test finishes, ITSDAQ generates files with the results. To understand these results, we need to introduce some concepts:

- The threshold is the minimum voltage at which a signal is labeled as a hit. A threshold scan consists of repeating the same type of test at different threshold values.
- The efficiency is the number of hits recorded as a signal over the total number of events recorded by the module. For very low thresholds noise will be counted as a hit, and for too high thresholds the injected charge will not be seen as a hit. The plot obtained when a threshold scan is done for the efficiency values is called an S-curve.
- The Vt50 value is the threshold value at which 50% detection efficiency is recorded. The Vt50 depends on the injected charge

ITSDAQ can perform different types of tests. A 'Full Test' is defined as a specific set of tests that must be run during module electrical testing. There are two types of full tests: the nominal test in which the tests are run with the nominal voltage and current

values of the components, and a shunted test, where the limit over these values is removed to study the electronics' behavior. ITSDAQ can perform the following tests:

- AMAC IV: During this test, a Current-Voltage curve is recorded. To do this, the sensor is biased and the voltage is ramped up in steps of 10 V between 0 V and 550 V. The upper bound corresponds to the maximum operating voltage of a module at the end of the detection lifetime. The leakage current on the AMAC is recorded to study the possibility of having a breakdown on the module.

- Trim Scan: This test is always the first one performed after the AMAC IV. This test aims to tune the channel-by-channel threshold to ensure the uniform response of the chip.

- Strobe delay: This test is run to calibrate the charge injection delay with respect to the clock phase. Optimizing the delay ensures the chances of detecting the calibration pulse. In Fig.3.8 a comparison between two strobe delay tests recorded at Lund University is shown. In Fig.3.8a the result obtained is bad. The calibration is not correct as the charge does not have a clear time window. In Fig.3.8b the opposite result can be observed and the calibration is done successfully.

- Response curve: In this test, a threshold scan is performed for ten different values of injected charge. The charge is injected through the discharge of a capacitor. Then, the efficiency for each threshold scan is plotted, giving ten different S-curve as an outcome. The Response Curve is the function plotted using the Vt50 values obtained as a function of threshold. In addition, three module parameters can be calculated: the gain is calculated as the slope of the Response Curve. The output noise is the standard deviation of the fit performed on the S-curve. Lastly, the input noise is the output noise divided by the gain. In Fig.3.9 two tests performed at Lund University are shown. The test shown in Fig.3.9a corresponds to a bad test result. Some strips are labeled as "fail". Moreover, the values for different strips are spread, indicating that it was not properly calibrated. The opposite scenario is shown in Fig.3.9b. In this case, the results obtained were good as any region is labeled as "fail". It is also observed homogeneous results for the different strips.

- Noise Occupancy/pedestal scan: The noise occupancy is a threshold scan recorded without any charge injected. This test aims to measure the base noise level for different thresholds. This test is used for calculating the operational window of the module, see Chapter 4. In Fig.3.10 a comparison between two tests performed at Lund University is shown. In Fig.3.10a a bad result is shown. It can be seen how the noise levels are over one for each threshold value. However in Fig.3.10b it is shown how this values decrease as the threshold increases.

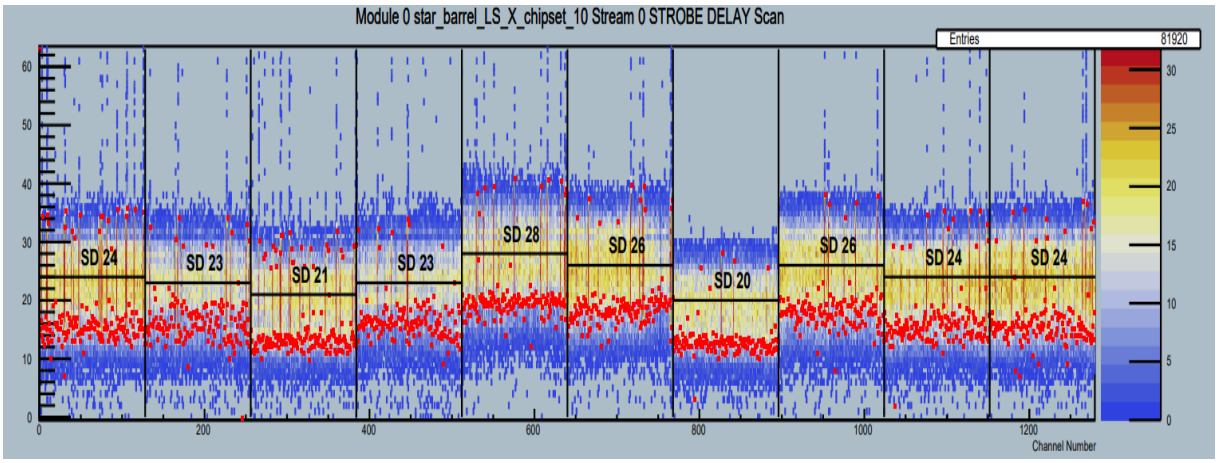

(a) Bad result from Strobe Delay test.

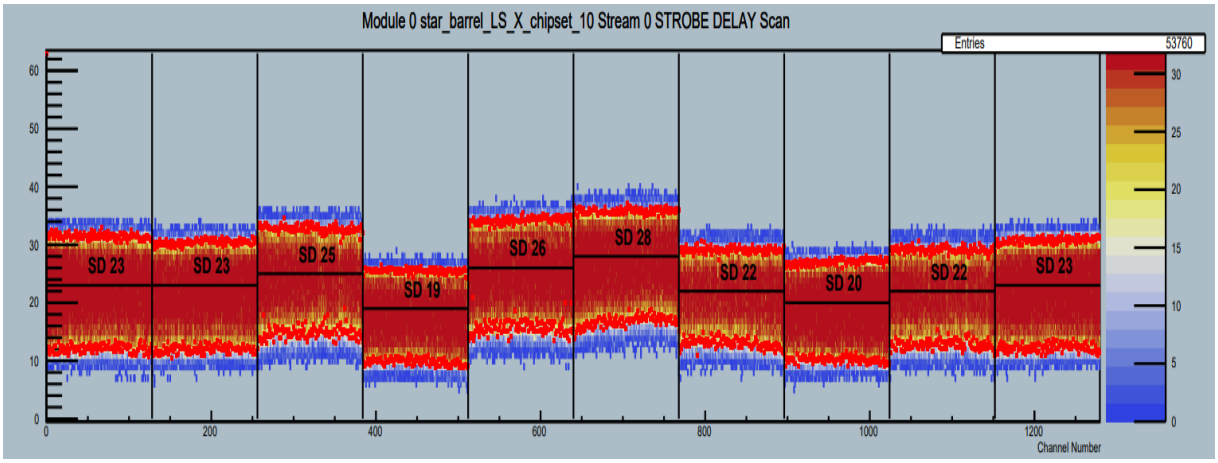

(b) Good result from Strobe test.

Figure 3.8. Strobe delay tests recorded at Lund University. a) The result of a bad strobe delay test is shown. There is no clear timing for the injected charge when it is always detected as a hit. b) The result of a good strobe delay test is shown.

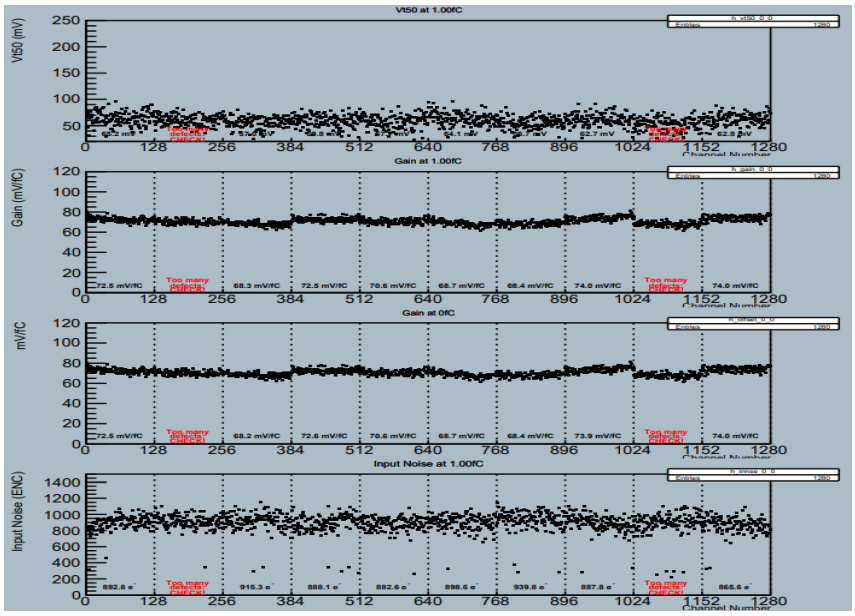

(a) Bad Response Curve test.

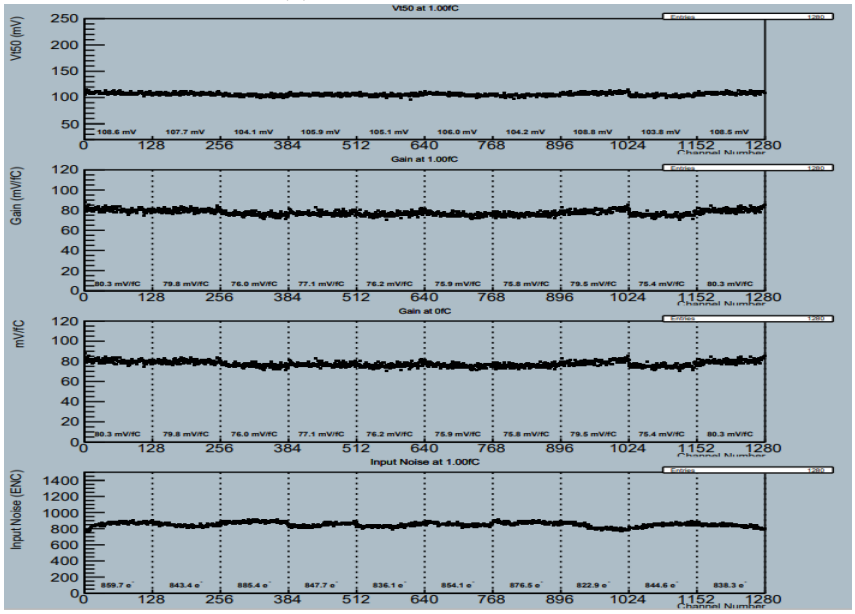

(b) Good Response Curve test.

Figure 3.9. Response Curve test results recorded at Lund University. a) We can observe 2 ABCs marked as fail. Moreover, a big spread between the data recorded in the strips. b) This is an example of a good test recorded. There are no strips labeled as "fail".

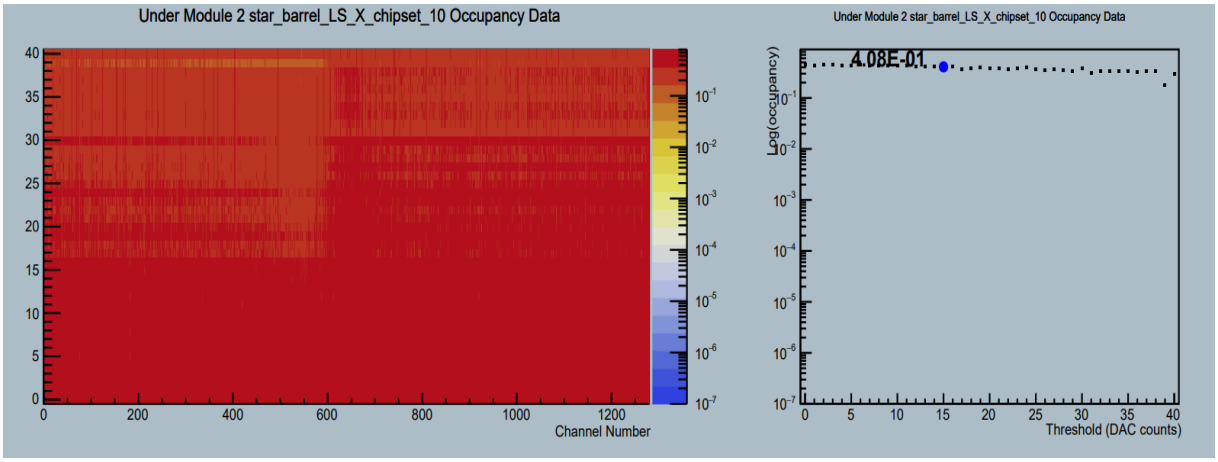

(a) Bad Noise Occupancy test.

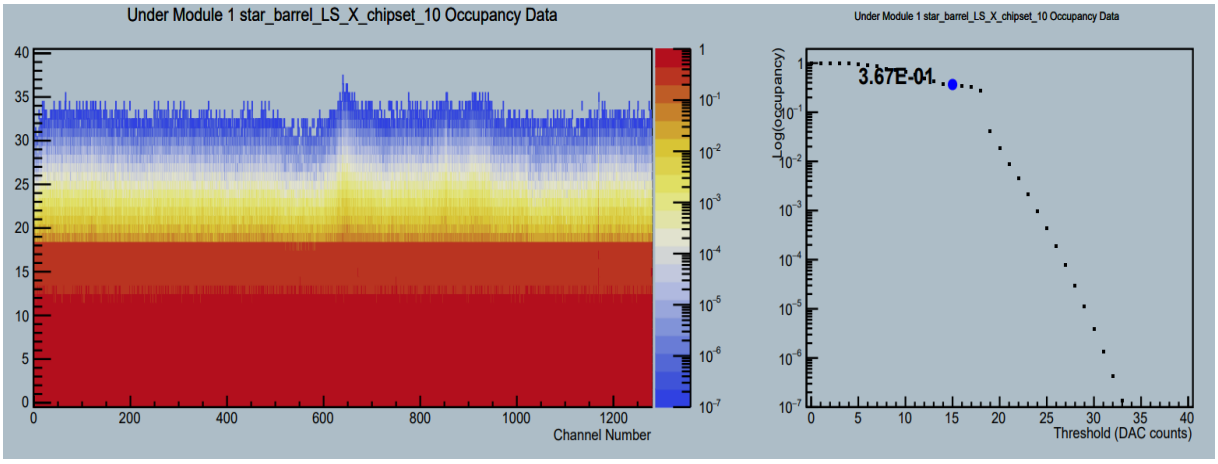

(b) Good Noise Occupancy test.

Figure 3.10. Noise Occupancy test results recorded at Lund University. a) The Noise Occupancy shown is an example of a bad result. The Noise Occupancy does not decrease with the threshold. b) The Noise Occupancy shown is an example of a good result. The Noise Occupancy goes to zero for the threshold between 30-35.

ITSDAQ and Coldjiglib communicate during the thermal cycle sequence, see Fig.9 from the appendix. Coldjiglib runs the thermal cycle sequence and whenever a test has to be performed, a message is sent to ITSDAQ. ITSDAQ sends a communication to Coldjiglib for the thermal cycle sequence to continue when it finishes the test.

3.4 Performing a Thermal Cycle

In this section, I will describe the process followed to perform a thermal cycle sequence. A thermal cycle sequence is divided into different sub-sequences: Pre-Cycling, Cold Characterization, Intermediate Thermal Cycles, Final Thermal Cycle, Post-Cycling, and Finish as can be seen in Fig.3.4. Coldjiglib will automatically set all the parameters, such as the chiller temperature, and will go through the thermal cycle sequence, see Fig.3.11.

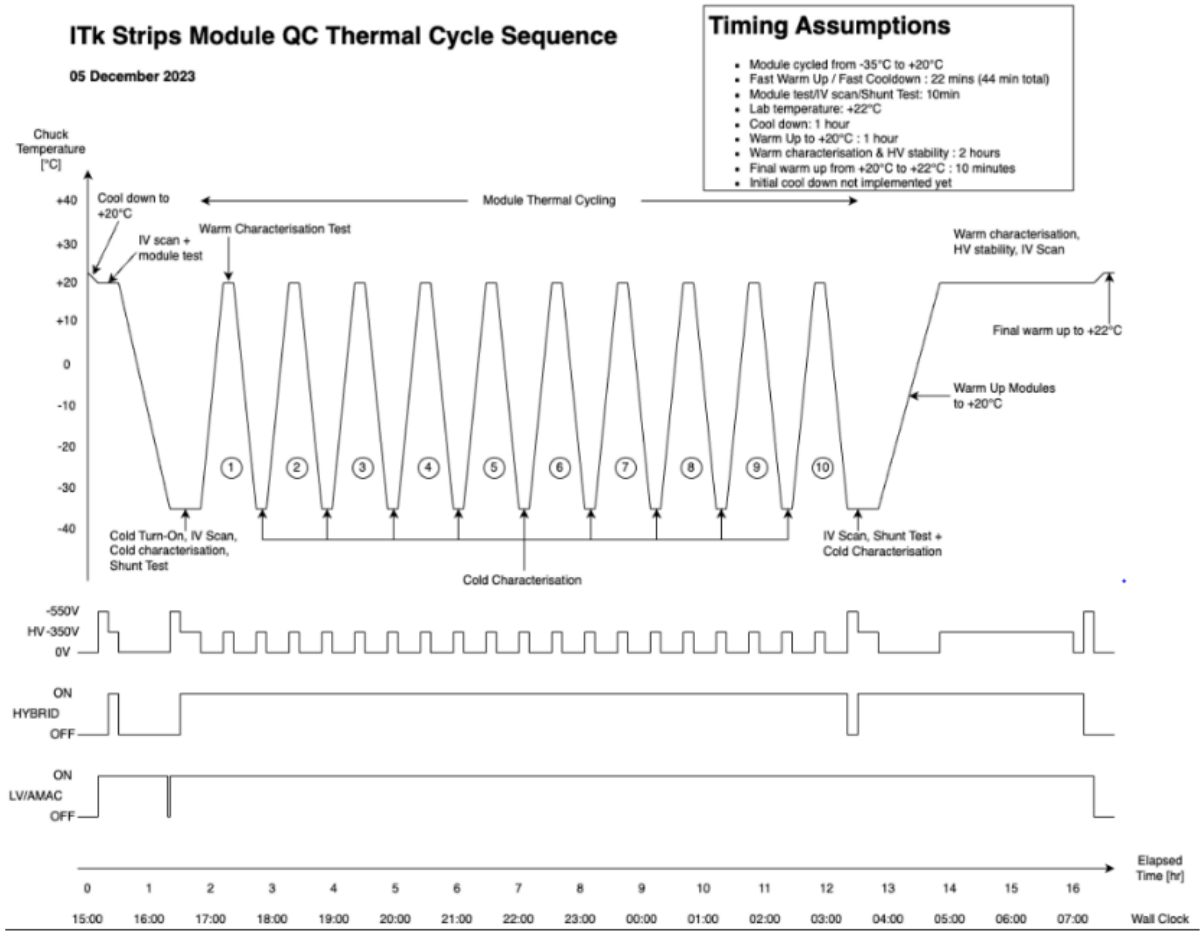

Figure 3.11. Ideal thermal cycle sequence [28].

The first step of thermal cycling is to place the module(s) on the chuck(s) and seal the Cold Box. Then, we establish communication with ITSDAQ. We run a quick test and check that the power supplies also respond. After this, we need to wait around one day for the RH inside the Cold Box to decrease. Typically the RH has to be lower than 0.5% to have a DP lower than -40 C.

The following day, we start the chiller, the GUI, ITSDAQ, and ITSDCS. The first step is to upload the correct information to the GUI about the modules under testing. Once this is done, we start the thermal cycle. The first sequence of the thermal cycle is the Pre-Cycling Sequence. This sequence ensures the connection between the module and ITSDAQ/ITSDCS works. If everything is working, Coldjiglib will set the temperature to $20°C$ to perform some tests on the modules. Starting with an AMAC IV, followed by a Full Test, and then a Shunted Full Test. The high voltage is always ramped down after the tests.

After this, Cold Characterization starts. The chiller starts to cool down to $-30°C$. The Peltiers turn on when the chiller reaches $-25°C$. Once the chucks under testing reach $-35°C$, the tests start. This part of the cycle consists of performing a full test on the module, as described in the previous sequence, while the temperature is kept at $-35°C$. In addition, a cold turn-on test is done to ensure the module can be turned on while it is cold.

After the full test is done, ITSDAQ sends a message to Coldjiglib to keep going with the TC and the Intermediate Thermal Cycles sequence starts. From this point on, cycling

starts. One cycle is considered going from $-35°C$ to $20°C$ and back to $-35°C$. A full test is performed each maximum or minimum. The Final Thermal Cycle sequence follows the last cycle. The modules are warmed up to $20°C$ and a shunted test is performed.

After the last warm-up is done, the temperature is kept at $20°C$, and the Post-Cycling Sequence starts. This sequence consists of keeping the high voltage on for two hours while the AMAC is read. This is also known as high-voltage stabilization.

After the high-voltage stabilization finishes, the modules are switched off, removed from the Cold Box and stored in the dry cabinet. The last step of the thermal cycle sequence is to upload the test results to the ITk database. In total, it takes around two days to perform a thermal cycle test. One day for reaching the desired humidity and one day for running the thermal cycle sequence.

Chapter 4

TestBeam

The motivation behind the test-beam campaign is to test modules under beam conditions to study their performance; particularly, efficiency and noise occupancy. In addition, the modules are under mechanical stress and operational conditions. This chapter discusses two test beam campaigns at DESY, Hamburg on the Test Beam Line 22 in December 2023 and March 204.

4.1 Testing Setup

The Test Beam Line 22 provides an electron beam of 5 GeV. The test beam setup consists of seven telescopes used for particle tracking. The modules are placed inside an environmental chamber, similar to the Cold Box, but designed for one module and the test beam setup. This chamber provides a support structure to place the module, establish communication with ITSDAQ, provide cooling, and record environmental data. The box has to be cooled down using dry ice to temperatures under $-40°C$. The dry ice is refilled whenever the temperature increases over $-40°C$.

In each campaign, different modules were tested. In the December 2023 campaig, a R0 module, R3 module, and SS module were tested. In the March 2024 campaign, three SS modules and one R0 were tested.

For every module, the testing procedure is the same. The module is placed inside the box and the communication with ITSDAQ is checked. Then, the box is cooled down and a hitting point for the beam is chosen. This is shown in Fig.4.1. After that, a pedestal scan is performed for different thresholds. When the pedestal scan finishes, the beam turns on, starting a threshold scan. When this process finishes, the point where the beam strikes the module changes, and another threshold scan is taken. This procedure is repeated at room temperature.

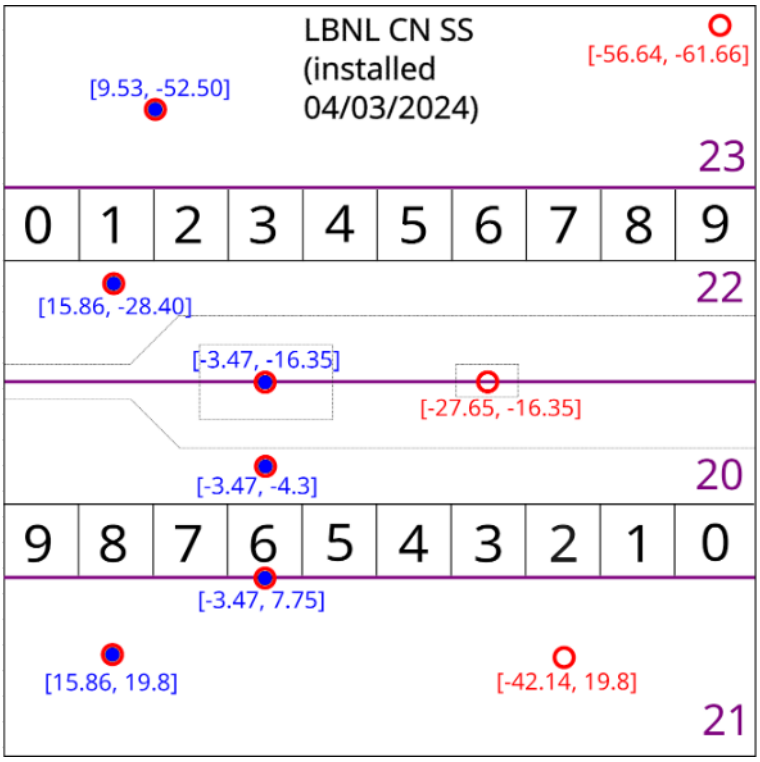

Figure 4.1. Scheme of the hitting points during the data taken of the SS module at the March 2024 test beam campaign [31].

There are three different types of modules suitable for testing: unirradiated modules, irradiated modules, and Cold Noise modules. The unirradiated modules have not undergone an irradiation campaign. Irradiated modules have undergone an irradiation campaign. Cold Noise modules are a special type of modules that have shown the so-called Cold Noise. Cold Noise is a phenomenon that consists of registering higher noise occupancy levels when the module is cold. This phenomenon is shown on strips close to the powerboard and the hybrids. Cold Noise seems to be related to the glue used during the manufacturing phase.

The hitting points are chosen in relation to the module that is under testing. In the case of irradiated and unirradiated modules, the points chosen are equally distributed along the module. The objective is to test the performance before and after the irradiation process. In the case of Cold Noise modules, the objective is to test the cold noise phenomenon and how it affects the performance of the module. Therefore, the points chosen focus on comparing the performance of Cold Noise regions with regions that do not show this phenomenon.

4.2 Analysis procedure

The analysis aims to find the operational window of a module's region. The operational window has to fulfill the following requirements:

- The efficiency is higher than 99%
- Noise Occupancy (NO) is lower than 10^{-3}

The tracking analysis is done using EUDAQ2 [32] and Corryvreckan [33]. EUDAQ2 is a data acquisition software. Corryvreckan is a software designed for reconstructing the events recorded. Corryvreckan uses two files to reconstruct the data: A geometry file that stores the information about the setup and the modules under testing and a configuration file that defines the analysis performed by Corryvreckan.

The Noise Occupancy is calculated using EUDAQ2 with the data recorded in the pedestal scans. Different pedestal scans are recorded, each of them with a different threshold. EUDAQ2, through the ItsOcupanccyScanner function, calculates the Noise Occupancy per strip. It also calculates the average noise occupancy in a defined region of strips. These strips are the ones hit by the beam.

The efficiency is calculated using Corryvreckan with the data recorded in the efficiency threshold scans. The efficiency is defined as the fraction of events detected over the total number of events striking the module. The procedure for calculating the efficiency consists of two parts: alignment and computing the efficiency. The alignment procedure is divided into: searching for correlations, pre-alignment, and alignment. The alignment process is done at a software level to obtain higher precision in the module placement. During the alignment procedure, Corryvreckan updates the geometry file with the new coordinates of the setup.

The first step of the alignment consists of finding correlations between the module and a reference plane. The telescope placed in front of the module defines the reference plane. Through this process, we can know how well-aligned the module is related to the telescopes. Moreover, this process ensures that the module and the data-taking process are working properly.

Once correlations are confirmed, we can run Corryvreckan in the pre-alignment mode [Prealigment]. In this mode, Corryvreckan will perform a translational shift of the module's coordinates in the geometry file. Corryvreckan analyzes the correlations found and shifts the module to center the correlations around zero. This process is run two to three times until the correlations are centered.

When the Pre-alignment procedure is finished, Corryvreckan is set in alignment mode [AlignmentDUT-Residuals]. This mode performs rotational and translational shifts of the module coordinates. To run this mode, the [DUTAssociation] and the [Tracking4D] are also activated. To perform the alignment, Corryvreckan calculates the differences between the predicted location of where the tracks intersect the plane and the real intersection point. The coordinate shift is performed to minimize this distance.

Once the alignment is done, efficiency can be calculated. To do this, Corryvreckan is run in the analysis mode [AnalysisEfficiency]. To calculate the efficiency, only events with one track are considered, hence the [FilterEvents] mode is activated. Corryvreckan provides the efficiency per strip and the average efficiency of the strips that have been fired during the data-taking.

Chapter 5

Results

5.1 Thermal cycle results

A full thermal cycle was performed between the 8th and 9th of April 2024, where R5 module received from IFIC was tested. The module was placed on chuck number four. This test aimed to ensure that we could perform a thermal cycle sequence. The thermal cycle sequence took approximately 20 hours. In Fig.5.1, the chuck temperature during the thermal cycle is shown. We did not observe any temperature deviation during the thermal cycle sequence. The temperature gradient never exceeded the $2.5°C/min$ required, as every half cycle took about half an hour for a temperature change of $55°C$.

Figure 5.1. Temperature recorded during the thermal cycle performed on the 9th of April. The dashed lines indicate the temperature measured in the copper part of the chuck. The dotted lines indicate the temperature in the aluminum. The temperatures on chuck number four are plotted in orange.

It is also important to analyze the cooling stress of the Cold box during the thermal cycle sequence. The chiller and Peltier's behavior during the thermal cycle sequence is shown in Fig.5.2.

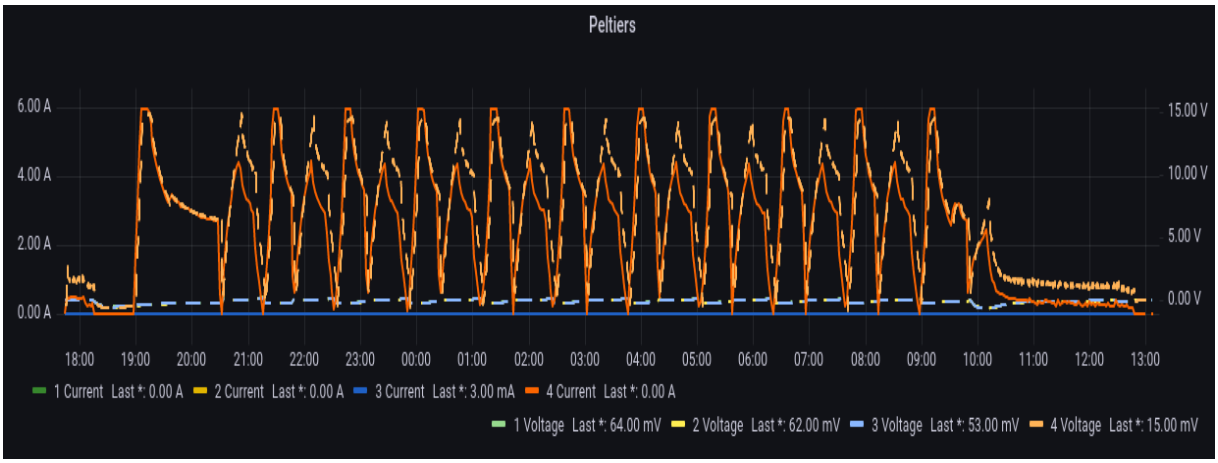

(a) Peltier plates voltage and current during the thermal cycle sequence.

(b) Chiller temperature during the thermal cycle sequence.

Figure 5.2. a) Peltier plates' behavior during the thermal cycle sequence. The dashed line corresponds to the voltage while the dotted line corresponds to the current. b) Chiller's temperature during the sequence, in red the chiller temperature and in green the temperature set by Coldjiglib.

From Fig.5.2, we can study the cooling performance of the Cold Box and the stress suffered by the two cooling methods. The first conclusion obtained is that both methods worked as intended during the thermal cycle sequence. In the Peltier's case, we can observe two repeated peaks of different heights. The higher one corresponds to the cooling part of the cycle and the lower one to the heating part. The Peltier plate current reaches the set current limit of 6 A during the cooling stage, but this effect is not a problem as the maximum current established by the Peltier manufacturer is 10 A. Moreover, the maximum is only reached momentarily so the chiller can cope with the heat dissipated by the Peltier. For the chiller performance, we can observe that it worked as set by Coldjiglib as it follows the set temperature. However, at the beginning of the cycle, it takes time to reach $-30°C$. This is produced by the heat generated in the Peltier. It does not produce a problem as the temperature keeps decreasing until it reaches the set temperature.

Another important variable to study during the thermal cycle sequence is the dew-point. In Fig.5.3, we can observe how the dewpoint decreases as the temperature of the Cold Box decreases. The important part to notice is that it never exceeds $-40°C$, near

the temperature of the module. Therefore, the humidity conditions achieved in the Cold Box allow us to test the modules safely.

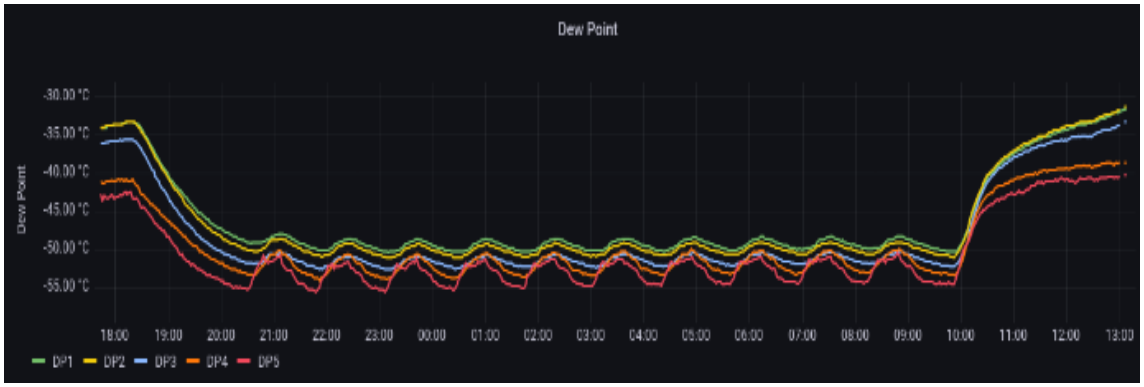

Figure 5.3. Dewpoint recorded during the thermal cycle performed on the 9th of April. The different lines correspond to the dewpoint calculated with the data measured by the RH sensors. The most interesting ones for this test are the orange one corresponding to chuck number four and the red one corresponding to the cold box air.

5.2 Test beam results

The data analyzed corresponds to the bottom left point in Fig.4.1 [15.86, 19.8]. This point is located in region 21 of an SS module. The threshold scan was run between 15 and 180 DAQ counts, with 400k events recorded per threshold. The noise occupancy scan was run between thresholds 0 and 50 DAQ counts. However, over threshold 50, the noise occupancy was 0, hence these data points were excluded from the plot. This module exhibits cold noise. The point under analysis is not located in a cold noise region. This is a control point. It is used to compare the operational window measure in the control region with the one measure in the cold noise-affected region. Therefore, calculating the operational window of this point is used to know how much the module's performance is affected by cold noise. The operational window found comprised between threshold 21 to 50. Comparing this operational window with the results obtained by Yajun He [34] or Alexandra Murphy [35] in cold noise regions, we can observe a larger operational window in the case of the point I analyzed.

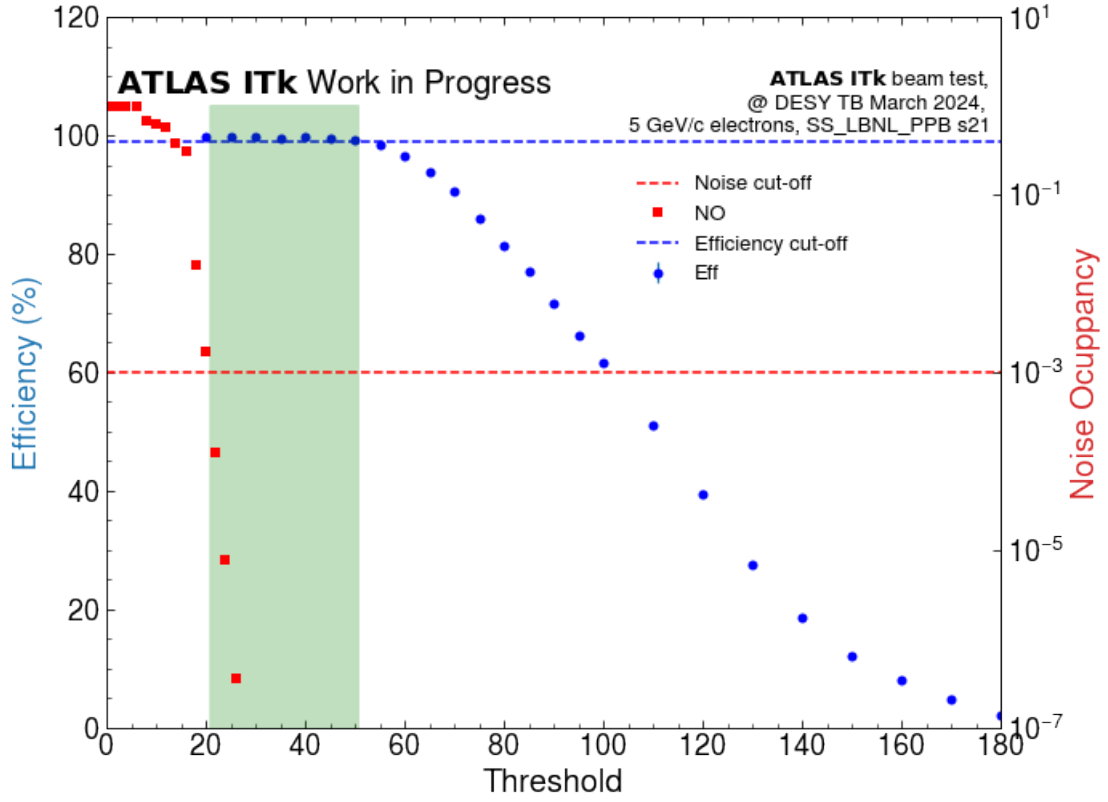

Figure 5.4. Analysis results for the CN SS module, point coordinates [15.86,19.8]. The S-curve is presented in blue. The noise occupancy scan is shown in red and the operational window calculated is shown in green.

Chapter 6

Conclusion and Outlook

The results shown during this thesis show that Lund University is prepared to perform thermal cycles. The Cold Box works according to the requirements established by the ITk collaboration for thermal cycling modules.In the next months, the ITK Strips collaboration will enter into the production phase, which will last approximately two years. The production phase will last approximately two years. During this time, Lund University is in charge of performing thermal cycling for 600 endcap strip modules. The commissioning of the Cold Box guarantees that Lund University is prepared for the production phase.

The production phase will be extremely challenging for the ITk Strips collaboration. As a testing site, Lund University must be prepared to cope with the number of modules produced at building places such as IFIC and DESY. A malfunction of the Cold Box could cause delays in module testing, leading to more delays in the production chain. For this reason, it is important to commission the Cold Box and understand how it works and how to perform maintenance work.

Bibliography

[1] Bernard Pullman. *The atom in the history of human thought*. Oxford University Press, USA, 2001.

[2] Ion CERNICA and Victor PASINCOVSCHI. "FROM ANCIENT ATOMISM TO FIRST KINETIC THEORIES OF GASES". In: ().

[3] Sylvia Berryman. "Ancient atomism". In: (2005).

[4] Andrew G Van Melsen. *From atomos to atom: The history of the concept atom*. Courier Corporation, 2004.

[5] M Gell-Mann. "Gell-mann 1964". In: *phys. lett* 8 (1964), p. 214.

[6] Richard E Taylor. "Deep inelastic scattering: The early years". In: *Reviews of Modern Physics* 63.3 (1991), p. 573.

[7] Joseph Incandela, on behalf CMS Collaboration, et al. "Status of the CMS SM Higgs search". In: *CERN Public Seminar, CERN, Switzerland*. 2012.

[8] CERN collaboration. *Large Hadron Collider*. Accessed on April 15, 2024. URL: `https://home.cern/science/accelerators/large-hadron-collider`.

[9] Thomas Schörner-Sadenius. "The large hadron collider—background and history". In: *The Large Hadron Collider: Harvest of Run 1*. Springer, 2015, pp. 1–26.

[10] CERN collaboration. *High-luminosity LHC*. Accessed on April 18, 2024. URL: `https://home.cern/science/accelerators/high-luminosity-lhc`.

[11] Stephane Fartoukh, Ilias Efthymiopoulos, Rogelio Tomas Garcia, Roderik Bruce, Helga Timko, Gianluigi Arduini, Nicolas Mounet, Yannis Papaphilippou, Benoit Salvant, Stefano Redaelli, et al. *LHC configuration and operational scenario for run 3*. Tech. rep. 2021.

[12] CERN collaboration. *CERN*. Accessed on April 12, 2024. URL: `https://home.cern/`.

[13] Chris Llewellyn Smith. "Genesis of the large hadron collider". In: *Philosophical Transactions of the Royal Society A: Mathematical, Physical and Engineering Sciences* 373.2032 (2015), p. 20140037.

[14] Ewa Lopienska. *The CERN accelerator complex, layout in 2022*. Tech. rep. 2022.

[15] Giorgio Brianti. "The large hadron collider project: historical account". In: *Physics reports* 403 (2004), pp. 349–364.

[16] O Brüning, H Burkhardt, and S Myers. "The large hadron collider". In: *Progress in Particle and Nuclear Physics* 67.3 (2012), pp. 705–734.

[17] ATLAS collaboration et al. *Expected performance of the ATLAS detector at the High-Luminosity LHC*. Tech. rep. ATL-PHYS-PUB-2019-005, 2019.

[18] ATLAS collaboration. *Luminosity*. Accessed on April 17, 2024. URL: https://atlas.cern/Glossary/luminosity.

[19] *Standard Model Summary Plots October 2023*. Tech. rep. All figures including auxiliary figures are available at https://atlas.web.cern.ch/Atlas/GROUPS/PHYSICS/PUBNOTES/A PHYS-PUB-2023-039. Geneva: CERN, 2023. URL: https://cds.cern.ch/record/2882448.

[20] Hermann Kolanoski and Norbert Wermes. *Particle Detectors: Fundamentals and Applications*. Oxford University Press, USA, 2020.

[21] CT Klein, LBA Hommels, V Fadeyev, D Gillberg, K Hara, JS Keller, T Koffas, J Kroll, SJ Lee, M Mikestikova, et al. "Initial tests of large format sensors for the ATLAS ITk strip tracker". In: *Nuclear Instruments and Methods in Physics Research Section A: Accelerators, Spectrometers, Detectors and Associated Equipment* 986 (2021), p. 164677.

[22] ATLAS collaboration et al. *Technical design report for the ATLAS inner tracker strip detector*. Tech. rep. LHC/ATLAS Experiment, 2017.

[23] Georges Aad, Xabier Sebastian Anduaga, S Antonelli, M Bendel, B Breiler, F Castrovillari, JV Civera, T Del Prete, Maria Teresa Dova, S Duffin, et al. "The ATLAS experiment at the CERN large hadron collider". In: (2008).

[24] Vincent Herberg. *ATLAS detector*. Accessed on April 24, 2024. URL: https://vincent-hedberg.web.cern.ch/atlas/atlas.html.

[25] *Expected tracking and related performance with the updated ATLAS Inner Tracker layout at the High-Luminosity LHC*. Tech. rep. All figures including auxiliary figures are available at https://atlas.web.cern.ch/Atlas/GROUPS/PHYSICS/PUBNOTES/ATL-PHYS-PUB-2021-024. Geneva: CERN, 2021. URL: https://cds.cern.ch/record/2776651.

[26] Sven Wonsak. "The ATLAS ITk Strip Detector System for the Phase-II LHC Upgrade". In: Feb. 2020, p. 017. DOI: 10.22323/1.373.0017.

[27] Pepe Bernabeu. *The ATLAS ITk Strip Detector for the Phase-II LHC Upgrade*. Accessed on May 13, 2024. URL: https://indico.tlabs.ac.za/event/112/contributions/2987/attachments/1155/1564/ATLASITkStripDetector-Bernabeu.pdf.

[28] Coldjiglib developers. *Internal communication inside the Cold Box community*. 2024.

[29] Alexander Ekman. "Searches for New Physics Using Innovative Data Acquisition, Analysis, and Compression Techniques". English. Defence details Date: 2024-05-17 Time: 13:00 Place: Rydbergsalen Name: Aarrestad, Thea Title: Doctor Affiliation: ETH Zurich —. Doctoral Thesis (monograph). Department of Physics, Apr. 2024. ISBN: 9789181040128.

[30] Robert Harry Hyde. "Growth and Characterization of Thermoelectric Ba 8 Ga 16 Ge 30 Type-I Clathrate Thin-Films Deposited by Pulsed Dual-Laser Ablation". In: (2011).

[31] Testbeam coordinators. *Internal communication inside the testbeam community*. 2024.

[32] EURDAQ2 community. *EUDAQ2*. Accessed on March 13, 2024. URL: https://github.com/eudaq/eudaq.

[33] Lennart Huth et al. *Corryvreckan*. Accessed on March 13, 2024. URL: `https://gitlab.cern.ch/corryvreckan`.

[34] Yajun He. *March 2024 test beam results*. Internal communication. Contact Yajun He for more information. 2024.

[35] Alexandra Murphy. *Silicon Strip Module Quality Control and Test Beam for the ATLAS Inner Tracker*. Bachelor thesis. 2024.

Appendix A

11.10 Module thermal cycling

As a part of the quality control portion of module testing, Lund will be receiving modules constructed primarily at Instituto de Física Corpuscular (IFIC), DESY, and Freiburg. Up to four modules at a time are to be thermal-cycled ten times between the temperatures of -35℃ and +20℃ , with an ITSDAQ “full test” to be performed at each minimum and maximum temperature and a two-hour high-voltage stability test at room temperature at the end of the thermal-cycles. The results of these tests are then uploaded to the production database and the modules are sent to IFIC, DESY, or Freiburg to be loaded onto a petal.

The Endcap cold-box makes use of a recirculating chiller and Peltiers to achieve the desired temperatures. Temperatures of metal surfaces are measured using NTC thermistors, and HYT939 sensors measure the temperature and relative humidity of the air. A Raspberry Pi controls the chiller, Peltier power supplies, and lid lock, as well as reads in sensor data to be sent to an Influx database. Coordination between the thermal cycling and the tests performed on a separate PC with ITSDAQ are handled via flags sent-to and read-from this database.

There are still aspects of thermal cycling that are still under development in the ColdJigLib community at the time of this writing. The documentation here will reflect this.

Logistics

Lund can support cycling up to four modules of any species simultaneously. [Caveat: There are special conditions for testing four R3 modules simultaneously. We are aware of and following those discussions in the Strips community.]

As a thermal cycling site:

LU will receive modules from IFIC, DESY, and Freiburg for thermal cycling. The exact rate is currently under discussion, but it is expected to be low. We plan to perform the electrical reception tests on modules in the cold-box. A typical week could look like:-

- Day 1: Receiving modules from a European endcap module building site, and completing all their reception tests (visual, electrical)
- Day 2: Thermal-cycle modules (partial occupancy in the box)
- Day 3: Ship to loading site

Alternatively, we could wait to fill our box and cycle four modules at a time. We do have the required dry storage available to accommodate this. We believe it is better to forward modules to loading sites more frequently.

As we have one box and low rates, we do not expect to run multiple boxes in parallel and expect to operate the box primarily during working hours.

As a long-term reliability testing site:

Metea Marr (SFU), Erik Wallin (LU), and Adib Shaker (LU) are developing a long-term reliability testing protocol. Either Lund or NBI may become a permanent long-term reliability testing site through Production. In that case, one of the two cold-boxes would handle the full module thermal load per week while the other handles the long-term reliability testing. Currently, we plan to run the box at half capacity (two modules per cycle).

Personnel

Under Swedish employment law, temporary personnel cannot be hired longer than one year. If we employed traditional technicians, we would have to rotate our workforce annually, which would mean constantly retraining personnel. On the other hand, doctoral students in Sweden can be compensated (both financially and via extension to their doctoral clocks) for their time invested in "duties for the department" outside their research work. We have secured assurance from both the Swedish funding agency, Vetenskapsrådet (VR), and the university that we may employ and compensate our doctoral students to operate the cold box. The same set of doctoral students are available for the full duration of the construction period. Two doctoral students are already actively engaged in commissioning and operating the cold box.

Testing Software and Hardware

Lund hosts the endcap cold-box designed by DESY. The manual can be found here on EDMS. The majority of contents of this document will refer to the components outside of the box, or customized material added to the box after delivery. For further information, please see the Twiki.

Computer Hardware and Software

Testing is performed in the cleanroom on a Dell precision 3650 running AlmaLinux (release 9.3 Shamrock Pampas Cat). The PC communicates with the Digilent 410-316 Nexys Video FPGA via an ethernet connection and a USB connection is used to program the firmware, which was downloaded from Matt Warren's "Firmware Emporium". For the tests in this document we were using version nexysv_itsdaq_vb5fb_FDP_STAR, but have since updated to nexysv_itsdaq_FDP_STAR_vb67b (as of April 18, this is the latest release). The FMC-0514-DP (FMC-DP) board is mounted onto the FPGA, which can support testing for up to 6 modules. Module tests are performed using ITSDAQ (running master branch 527325fd7345d4796e46fd5e36ace6d36894c672 from March 28)

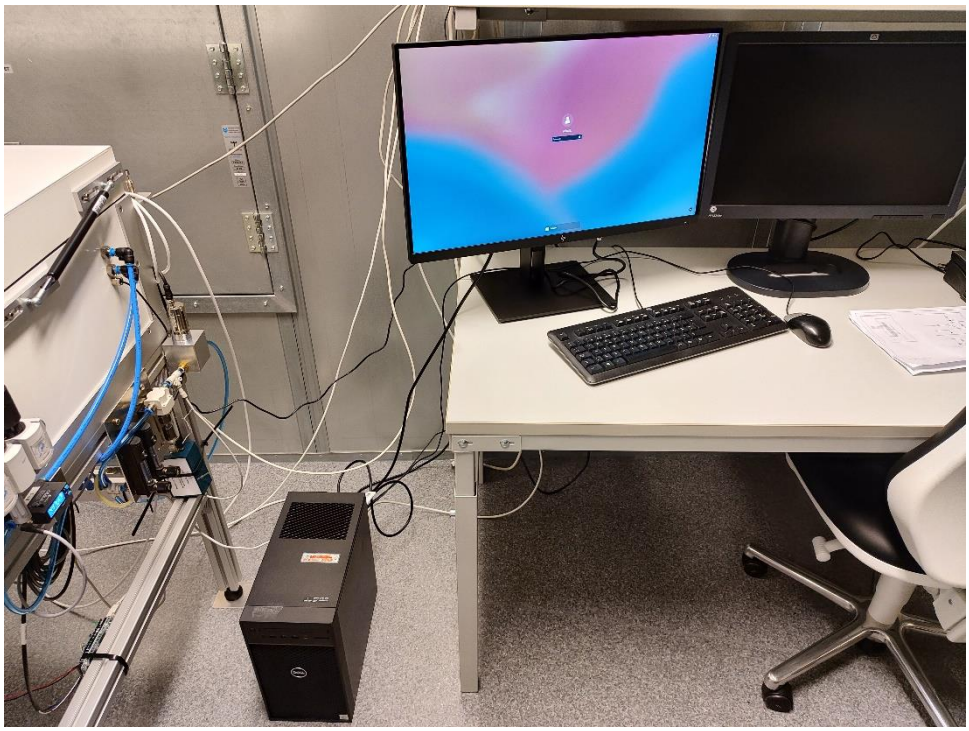

Figure 1: Picture of the PC and the CB operating place inside the clean room.

Power Supplies and Cabling

Module LV	4x TENMA 72-2705 programmable DC PS (30V, 3A)
Module HV	CAEN DT1415ET HiVolta
Peltiers	2x TTi CPX400DP (2 channels each)

Spare: Rhode & Schwar HMP4040 Programmable Power Supply 384W; 32V, 10A

High voltage is supplied to the modules using the Caen HiVolta DT1415ET 8-channel power supply. Communication between the Caen and the PC is via an USB cable. SHV cables are connected from the front of the Caen to the cold-box. The cable shields are separated such that the end connected to the PS has two SHV cables, with the center wire of one connected to the "+" terminal, and the other the "-" terminal (with the cable's ground shield floating) to provide a negative bias voltage to the sensors, as this model only ramps to positive voltages. The compliance current depends upon which endcap module is installed, but this typically ranges between about 40 uA and 100 uA, and automatically set by ITSDAQ.

Low voltage is supplied to each module via four TENMA 72-2705 power supplies (PS). Banana patch cables are connected to each of the outputs on the LV PSs and are connected to the cold-box. Communication between the TTi and the PC is via an USB cable. The low voltage is set to 11V with a compliance of 1.2A.

The Peltier elements are powered by two TTi CPX400DP (2 channels each) power supplies which are plugged into the polarity switch before going to the cold-box. Communication between the TTi and Raspberry Pi (RPi) is via an USB cable. Compliance voltages are set in software, but typically are less than 30V to prevent damage to the Peltiers. Current is currently limited to 6.0A, but we can manage 8.0 A safely.

The 24V voltage supply used for the bypass valve and the interlock is the RND 320-KD3005p.

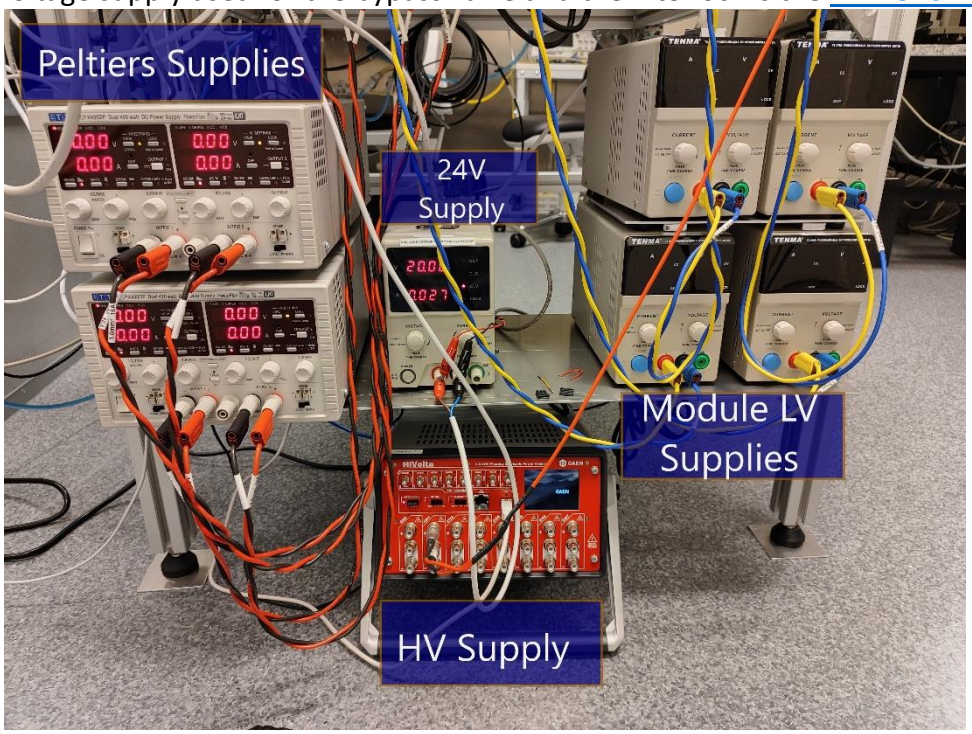

Figure 2: Picture of all the power supplies used in the set up.

Environmental Monitoring

The Endcap cold-box is designed to be controlled using a Raspberry Pi (RPi) and several pieces of custom and off-the-shelf hardware. Power distribution from the 24V supply is primarily handled by the custom PITk-board (from Lund) for the Pi, which also acts as a voltage divider for the NTCs. The divided output is connected to a series of analog pins in the DAQC2 Plate.

The temperature of the aluminum plate the module sits on, as well as the temperature of the copper chuck, are monitored using NTCs calibrated for the temperature range. Calibrations have been performed at Lund by Lennart Österman to determine a more-appropriate B-constant for our NTCs.

Air flow meter

The humidity inside the cold-box must be low and constant, hence it is necessary to inject dry air directly into the cold-box. It is also necessary to measure the amount of injected dry air. To do this, we use the Festoflowmeter. The Festoflow is connected to the Raspberry Pi using an ADC board. We made the connections through the BUS connection, following instructions from Cole Helling.

Chiller

We use the Grant TXF200 control box with R5 circulating bath (Grant-TFX-200R5) with silicone oil, Thermal C5, as the coolant. The coolant lines leading into the cold-box are ~1.5 - 2m and made of viton with basic insulation around the lines. In our case, the chiller is outside the cleanroom, to minimize noise and heat dumping into our (small) cleanroom.

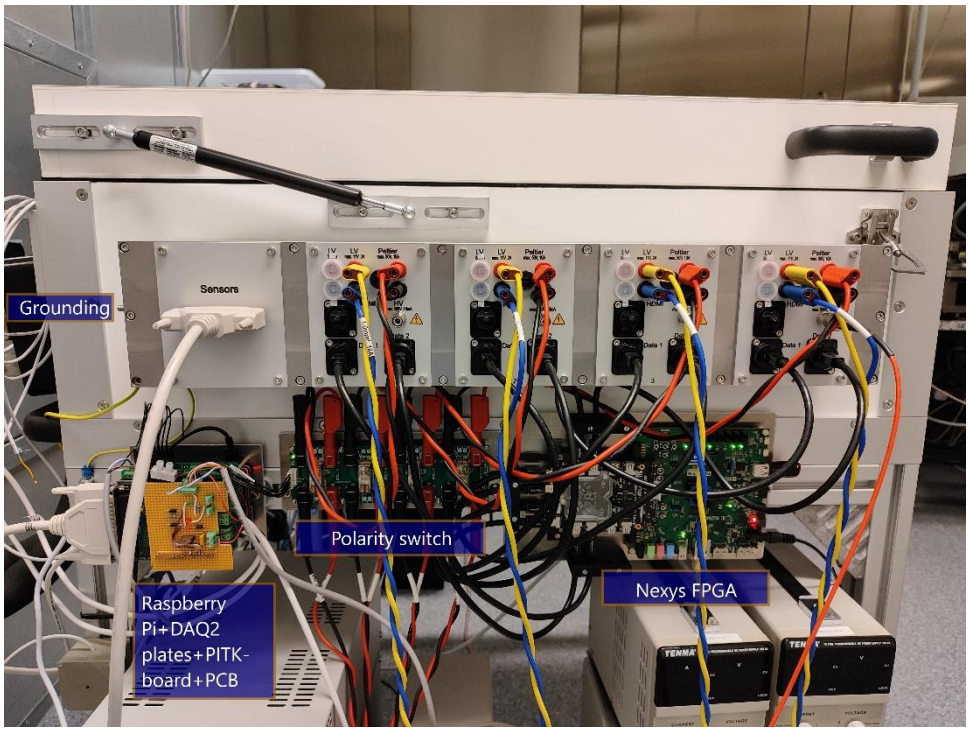

Figure 3: Picture of all the left side of the cold-box.

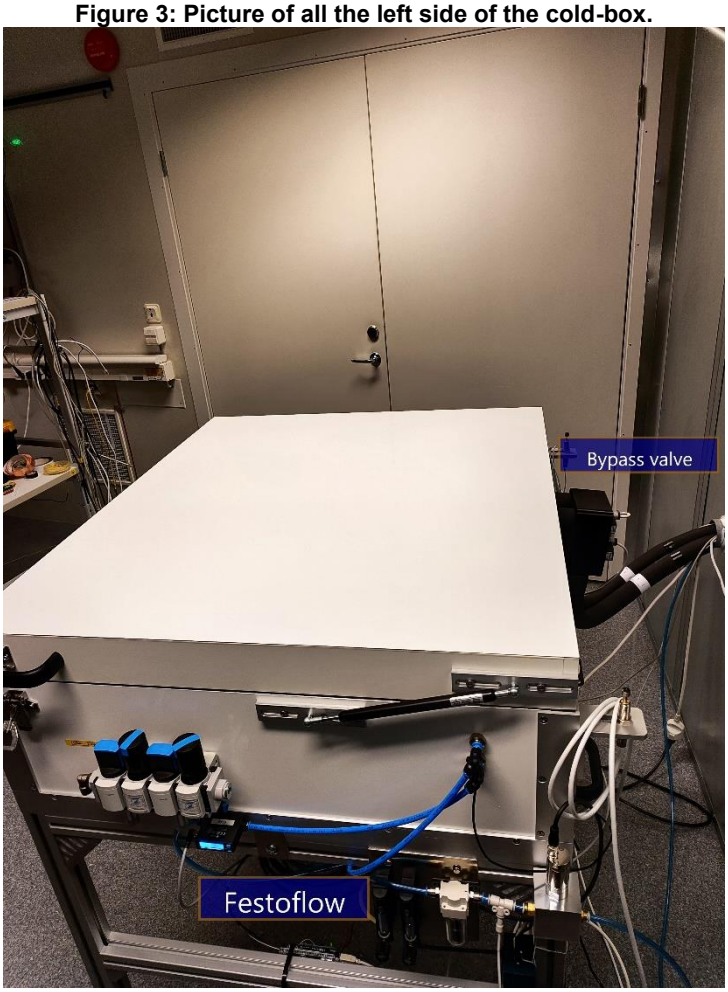

Figure 4: Picture of the right side of the cold-box.

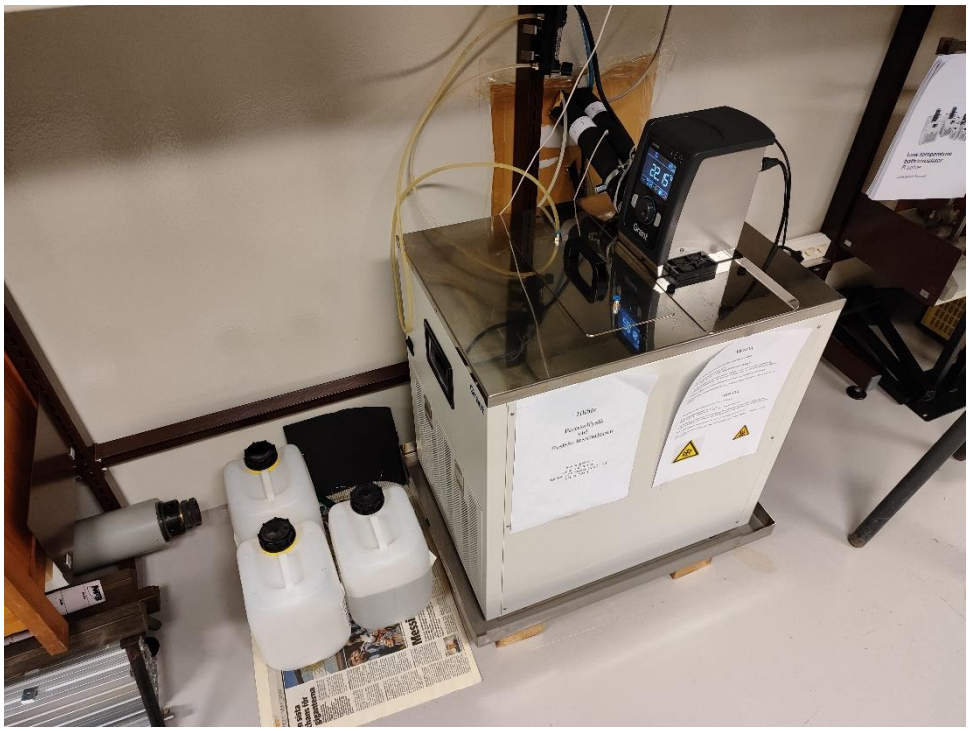

Figure 5: Picture of the Grant chiller with the silicone oil. The tubing passes through the wall into the cleanroom to minimize distance traveled.

Grafana Outputs

In what follows, we have several screenshots of our cold-box Grafana. Figure 5 shows the coldjig status panel. We are monitoring dewpoint (DP), air flow (Air), relative humidity (RH), lid interlock status (LID), temperature (TEMP), high voltage status (HV), Berstein lock (Lock), thermal cycling status (TC), bypass status (Bypass), and Peltier status (Peltier).

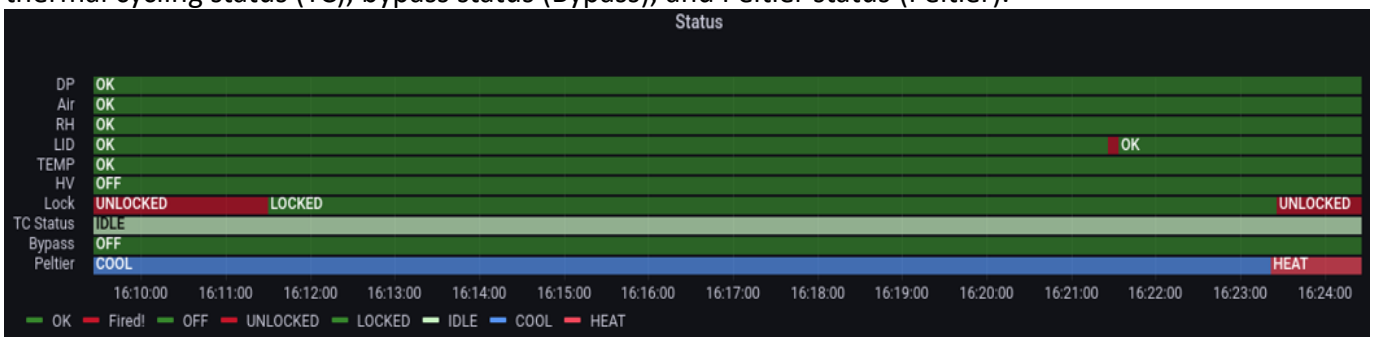

Figure 6: Screenshot of the coldjig status.

In the status panel, we can see the following indicators:

- Interlock Values. All of which are a boolean T/F, converted to OK and Fired in Grafana.
  - DP: [OK/FIRED]
  - Air: [OK/FIRED]
  - RH: [OK/FIRED]
  - LID: [OK/FIRED]
  - TEMP: [OK/FIRED]
- Other, optional, status information:
  - HV: [ON/OFF]
  - Lock: [LOCKED/UNLOCKED]

- TC Status [IDLE, TC_INITIALCOOLDOWN, TEST_START, etc]
- Cooling/heating related status information:
- Bypass [ON/OFF]
- Peltier [HEAT/COOL].

Figure 7: Screenshot of a few "global" parameters.

Figure 6 displays the Grafana display for global parameters:

- TC run number [int]
- TC cycle number [int]
- Chiller set, bath, and external-probe temperature [°C]
- Coldbox air temperature (general) [°C]
- Coldbox relative humidity (general) [°C]
- Air flow [L/min]

Figure 8: Screenshot of the overview panel.

Figure 7 shows the overview panel. The rows are all the same variable for each of the chucks. Going through columns from left to right, we have readout for:

- Chuck temperature gradient [°C/min]
- Chuck target temperature [°C]
- Aluminum plate temperature [°C]
- Copper Chuck temperature [°C]
- Dew Point [°C]
- Air temperature [°C]
- Relative humidity [%]
- PID mode [IDLE, INTERMEDIATE_HEATING, etc]
- Peltier current, voltage, and calculated power [A, V, W]

Figure 9: Screenshot of the commands send back and forth between ITSDAQ and coldjiglib.

Figure 9 shows the communication between ITSDAQ and the coldjiglib for a few exchanges.

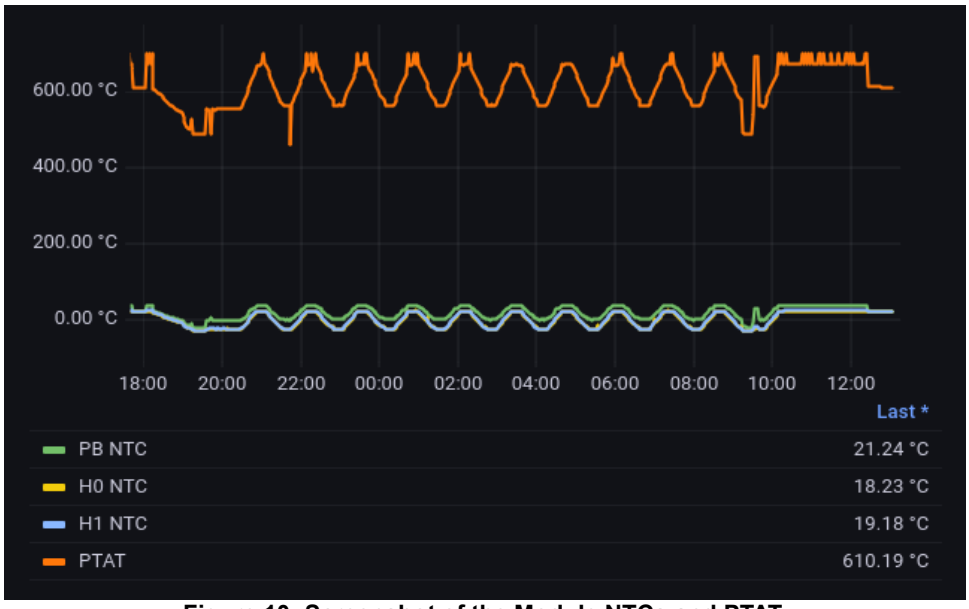

Figure 10: Screenshot of the Module NTCs and PTAT.

Interlock Features

The module thermal cycling system has several interlock features in software and hardware to keep modules and humans safe during operation.

Hardware Interlocks

Although not required, our setup has a HV interlock which uses the physical locking mechanism (which is also our lid switch) to force the Caen HiVolta into interlock when the box is opened. This is accomplished with a simple circuit (cartoon in figure 14).

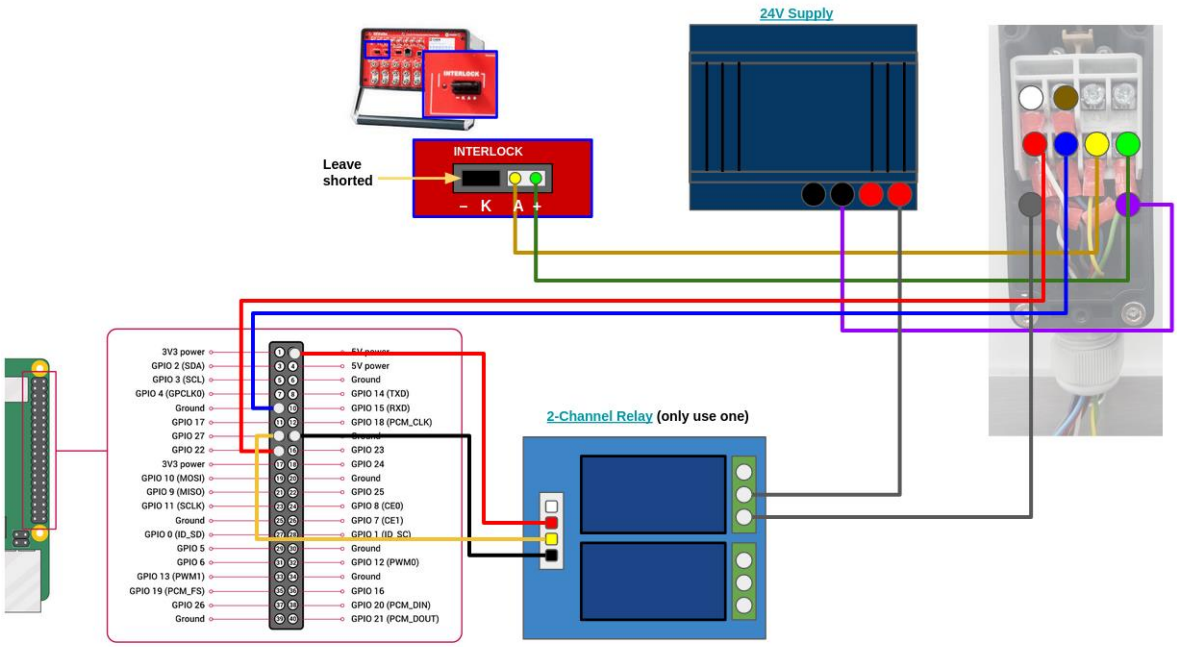

Figure 11: Basic cartoon diagram showing the connections for our physical interlock device for the HV Interlock and the controlling circuit to look/unlock the box. Designed by Cole Helling.

At Lund, we have adapted the design in figure 14 to our Clean room. We have designed a PCB (figures 15-16) where a transistor takes the role of the relay in Cole Helling's design. The next section shows how the interlock works.

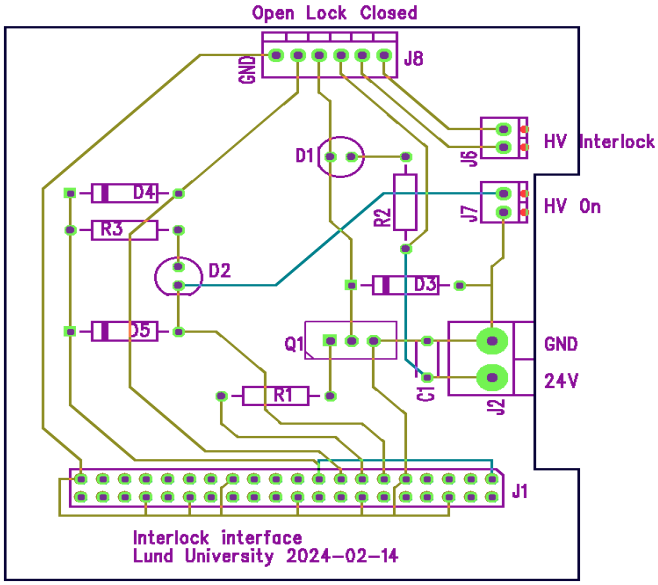

Figure 12: PCB´s design for the interlock feature. The PCB will be connected on top of the PITK-board.

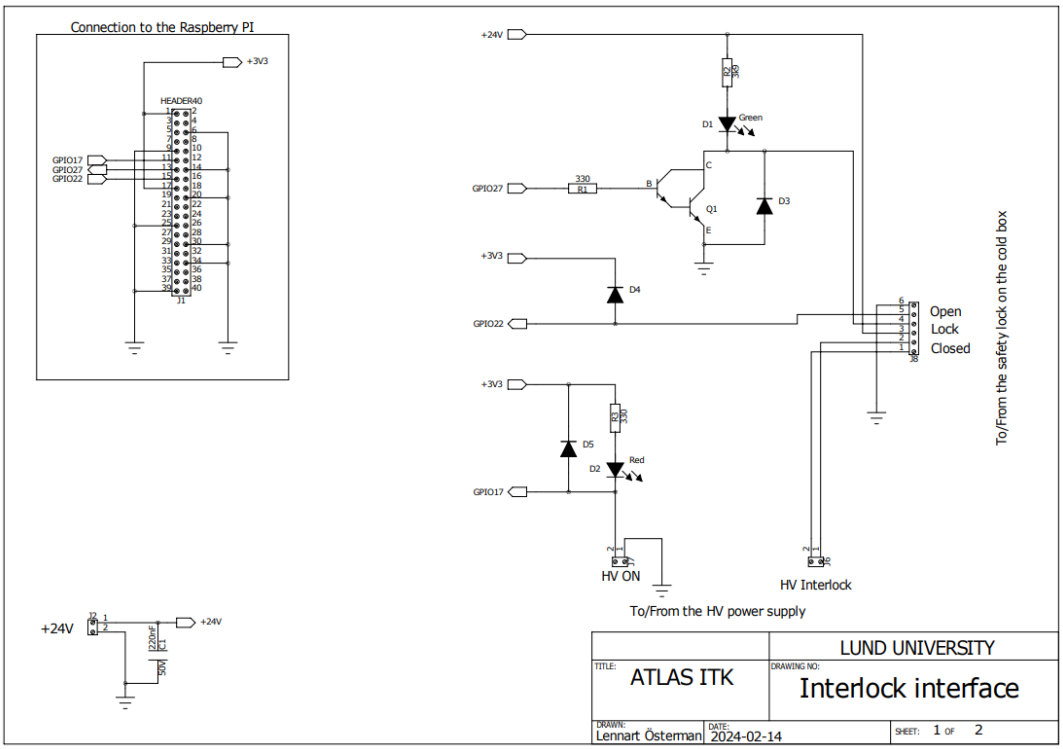

Figure 13: Schematics of the connections between the PCB, the Bernstein interlock and the HV supply.

Software Interlocks

All of the test shown are performed following Cole Helling guide: [Testing interlock]

Dewpoint and relative humidity interlocks

The first software interlock we will show is the dewpoint interlock. The relative humidity interlock functions the same way, so only the dewpoint interlock is discussed here. The dewpoint interlock trigger was hardcoded to 5 C so the interlock will fire if the temperature is less than 5C lower than the lowest temperature in the Coldbox. When fired, the interlock cuts the current activity, notes the fired trigger on the display panel (figure 14), and takes corrective action to return the cold box to a safe state.

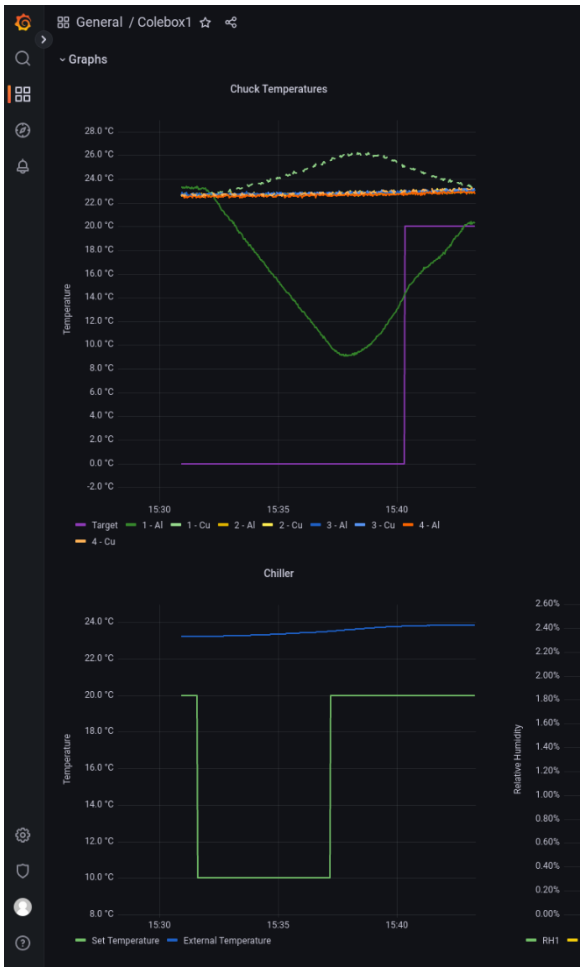

Figure 14: DP interlock firing (top), Corrective actions taken (bottom).

To test the dewpoint interlock, we programmed the box to cool to 10 C. Figure 14 shows the dewpoint interlock firing, changing the interlock status from “OK” to “Fired.” In response, the interlock software warmed the coldbox (bottom of figure 14) and updated the dewpoint interlock status to “OK.” The temperature then ramped up within the expected maximum rate of 2.5 ℃/min. We can see also that the chiller target temperature changed to 20 C.

Temperature interlock

Next is the temperature interlock. There are two possible temperature excursion on the coldbox, more than 30C and less than –45C. The latter is highly unlikely to happen so we will test the warm excursion. When this limit is surpassed the software takes corrective actions, chiller temperature and ramp down the peltiers current. We attempted to take the temperature up to 31 ℃, 1 ℃ above the maximum software limit. Shortly after reaching above 30C, the interlock fired and the software started to ramp down the current on the peltier supply, allowing the temperature to relax back down to a more reasonable temperature. The chiller was also set to 22 ℃ (the current “ending” temperature after cycling).

Figure 15: Interlock firing (top), temperature taking corrective action (bottom), as intended.

Lid switch interlock

The lid switch controls if the box is locked or unlocked. When we start the GUI, the coldbox locks and unlocks as part of the procedure. The coldbox it is locked whenever the temperature is lower than 15C (This can be seen in Fig 15) or the HV is on. For testing the lid interlock we started a cycle (only going to 10 ℃) when the temperature was lower than 15C the box was locked and when the coldbox reached the temperature we opened the LID. The LID was only open for a second, but enough to fire the interlock. Since the box was in the middle of a cooling phase, the peltiers were switched to heating mode to put the temperature back up to an acceptable level. In FIG XX, we can see how when the box is open the software carries the corrective action ramping up the temperature.

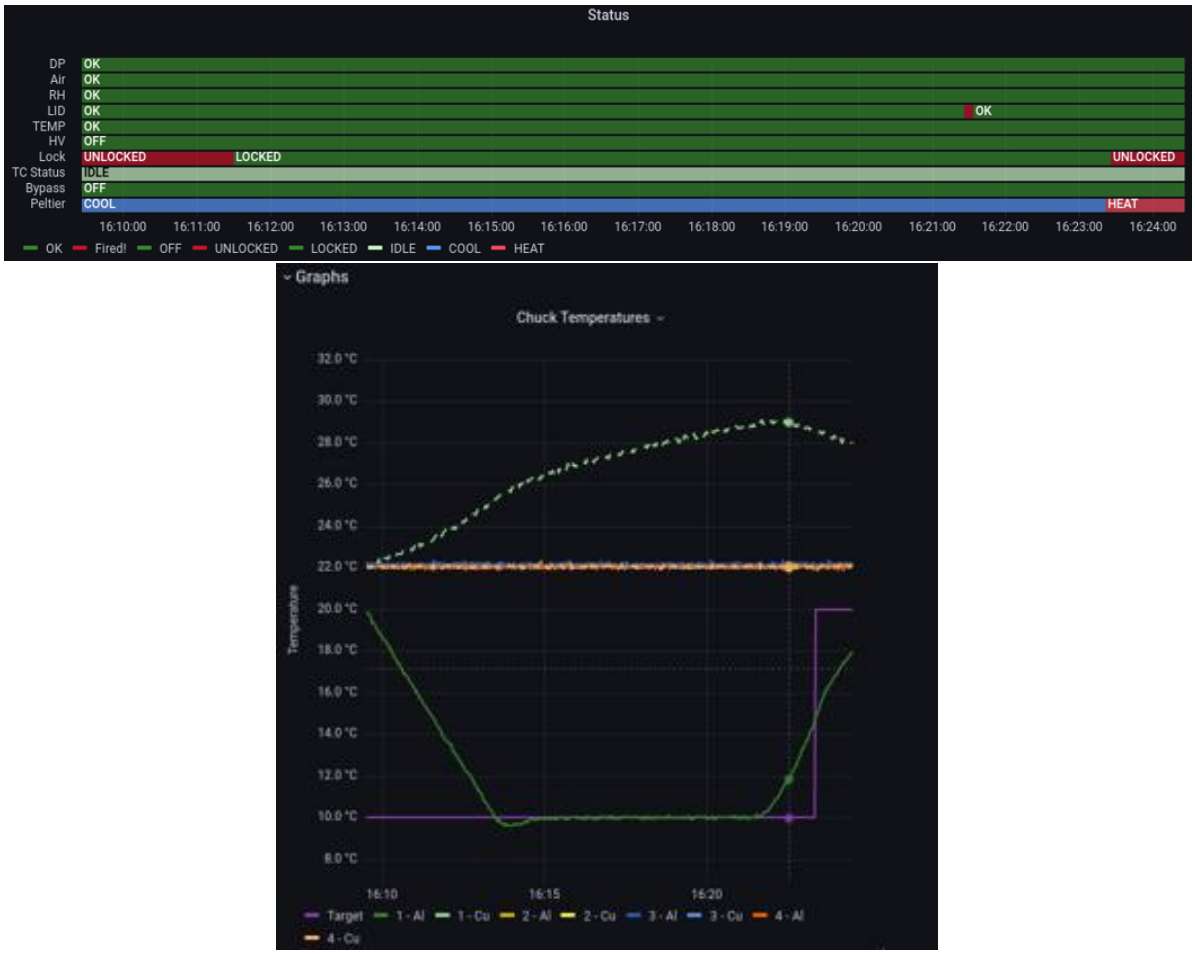

Figure 16: Interlock firing (top) and the corrective answer in the temperature(bottom).

HV interlock

The last interlock is the HV interlock. The coldbox is locked when the HV is on. For example during the HV stabilization at the end of a thermal cycle the coldbox is locked altough the temperature is higher than 15C . For this test, we connected the HV. Then, we opened the LID of the coldbox this action makes the HV to be turn off, we oppened the coldbox only for a fraction of a second but still we can observe how the HV switches off.

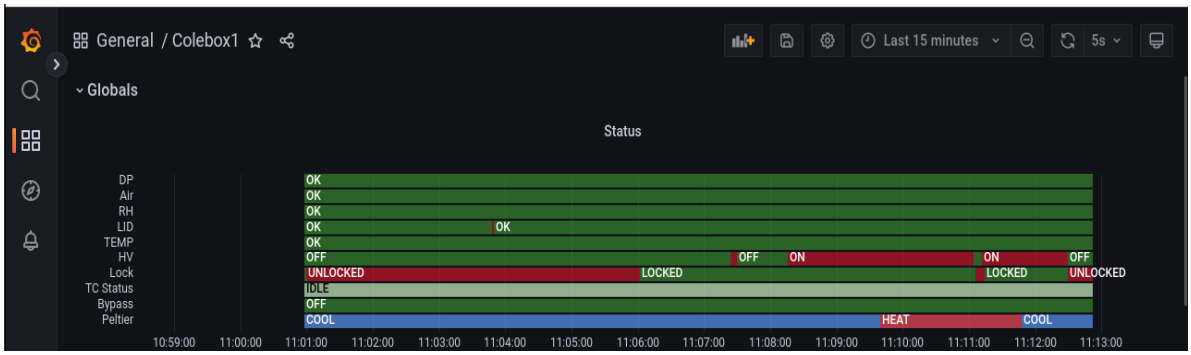

Figure 17: status after the test described.

We have also connected the Caen power supply's interlock for additional safety.

Coldbox grounding scheme

As every other EC coldbox, there is a system to ground the CB. In our case, we have ground the coldbox but also the structure under the box, as it can be see in Fig 18.

Figure 18: Grounding of the box.

Unloaded thermal cycling sequences run at Lund University

No modules, no external heat load on chucks

In our first set of tests, we cycled simultaneously all four chucks without modules to see that all chucks can reach the desired temperatures within a minute or so of each other and maintain that temperature with very little variance (usually 0.1 ℃).

Figure 11 shows the four chucks' temperatures during two cycles. We employed a twenty-minute wait at each achieved setpoint to simulate a test. The chucks started

warming at 12:40 and entered a “test” around 13:15 for a total of 34 minutes of temperature ramping (give or take a minute). Cooling began around 13:35 and another “test” began at about 14:13 for a total of 38 minutes of temperature ramping. So, we are staying within the “spirit” of a 1-hour cycle time.

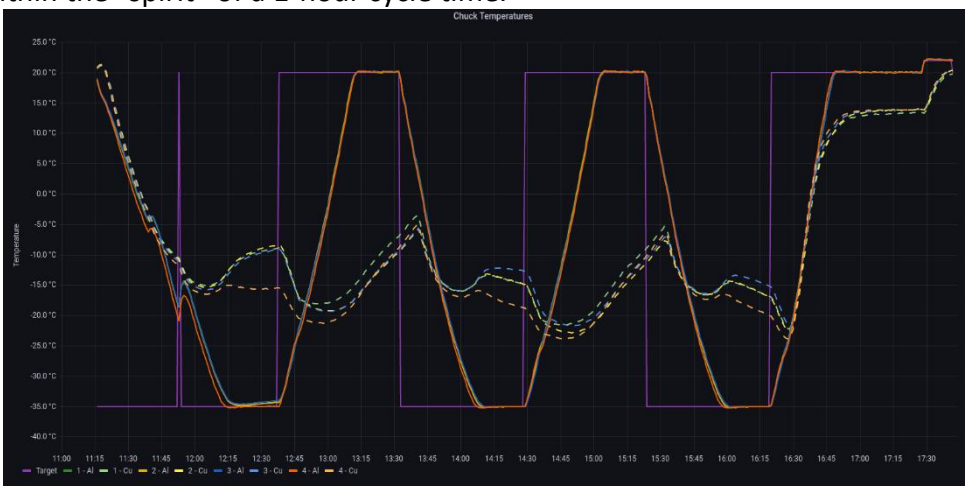

Figure 19: Screenshot of 4 chuck’s temperature throughout two cycles.

Figure 20 shows that we can do a full ten cycles in one go. The test took around 22 hours.

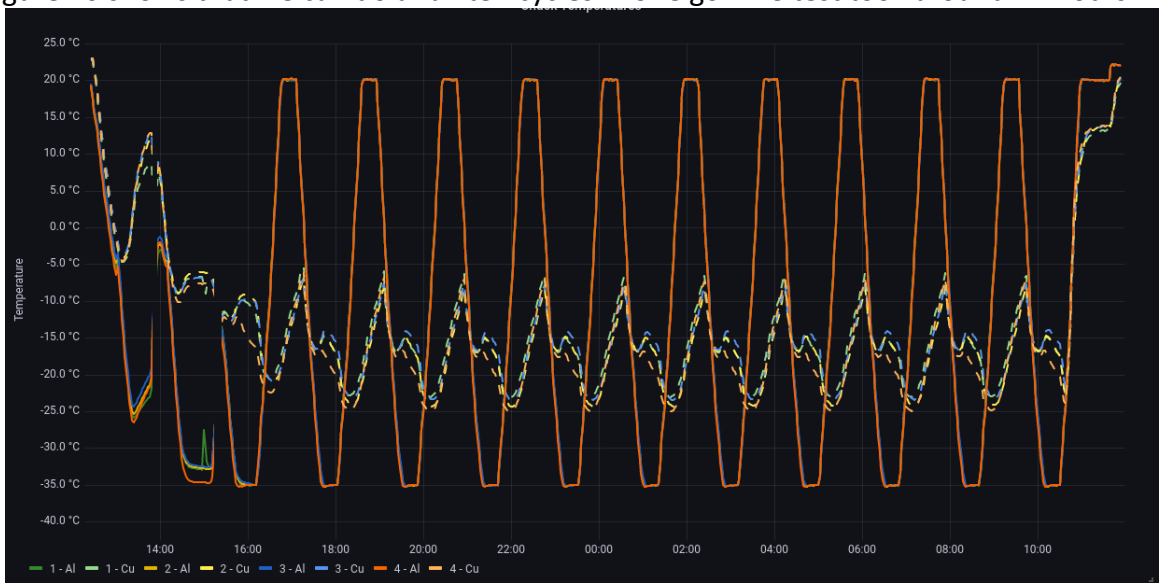

Figure 20: Screenshot of a cycling in one attempt.

Stress test with external heat load on all chucks.

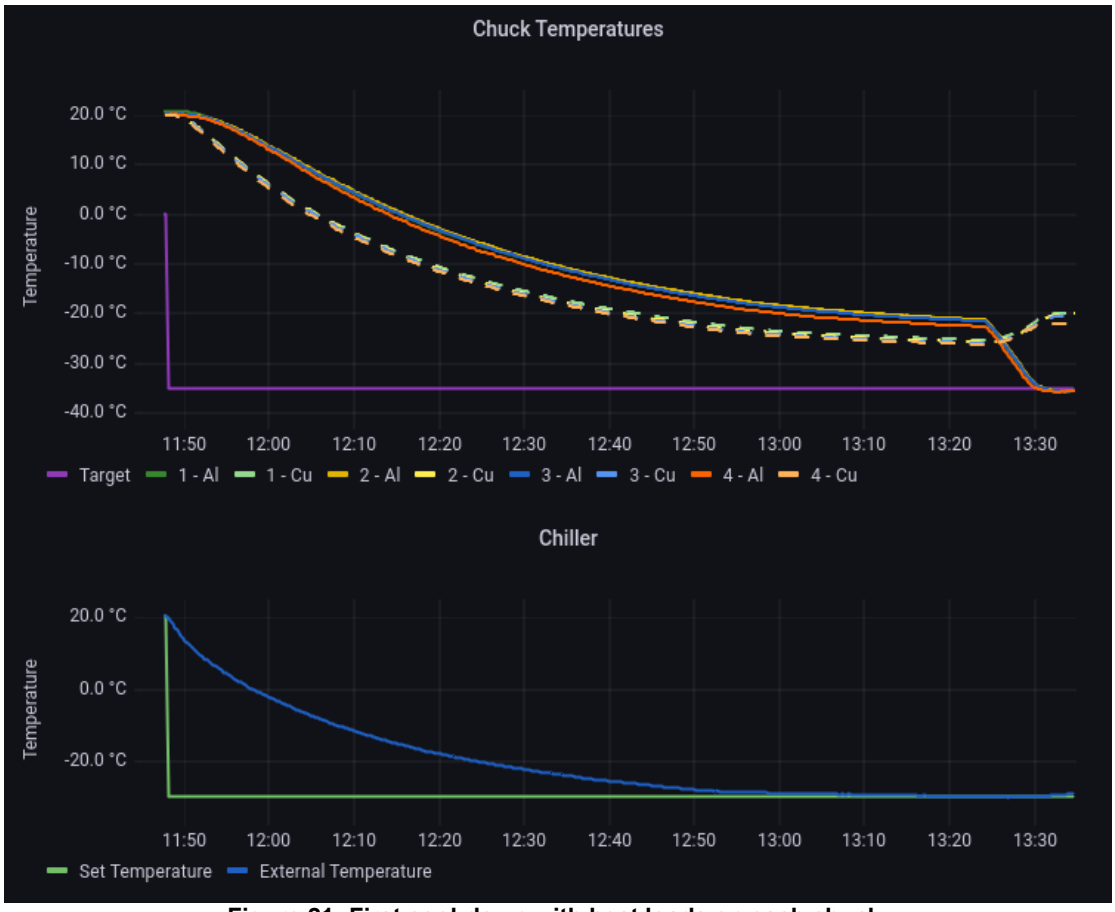

Figure 21: First cool-down with heat loads on each chuck.

Loaded Thermal cycling sequence: 10 cycles test with a module.

We made a full thermal-cycle sequence with a module loaded in the coldbox to check that everything is in place and we fulfill all the requirements. Figure 22 shows the Grafana output for this complete sequence.

Hardware initialization file and Influx configuration file

The Lund hardware configuration file can be found here.

St_system_config.dat file

```
DAQ udp 192.168.222.16 60001,60001
DAQ udp 192.168.222.16 60002,60002

Module   0  1  1   0  32  -1  25  25  ABCStar_R5H0_ppa R5H0
Module   1  1  1   0  34  -1  25  25 ABCStar_R5H1_ppa R5H1
```

Configuration files from individual modules

We did this test with a single module (give the ID of the PPA R5 here) using the default R5 config.

Images from loaded TC

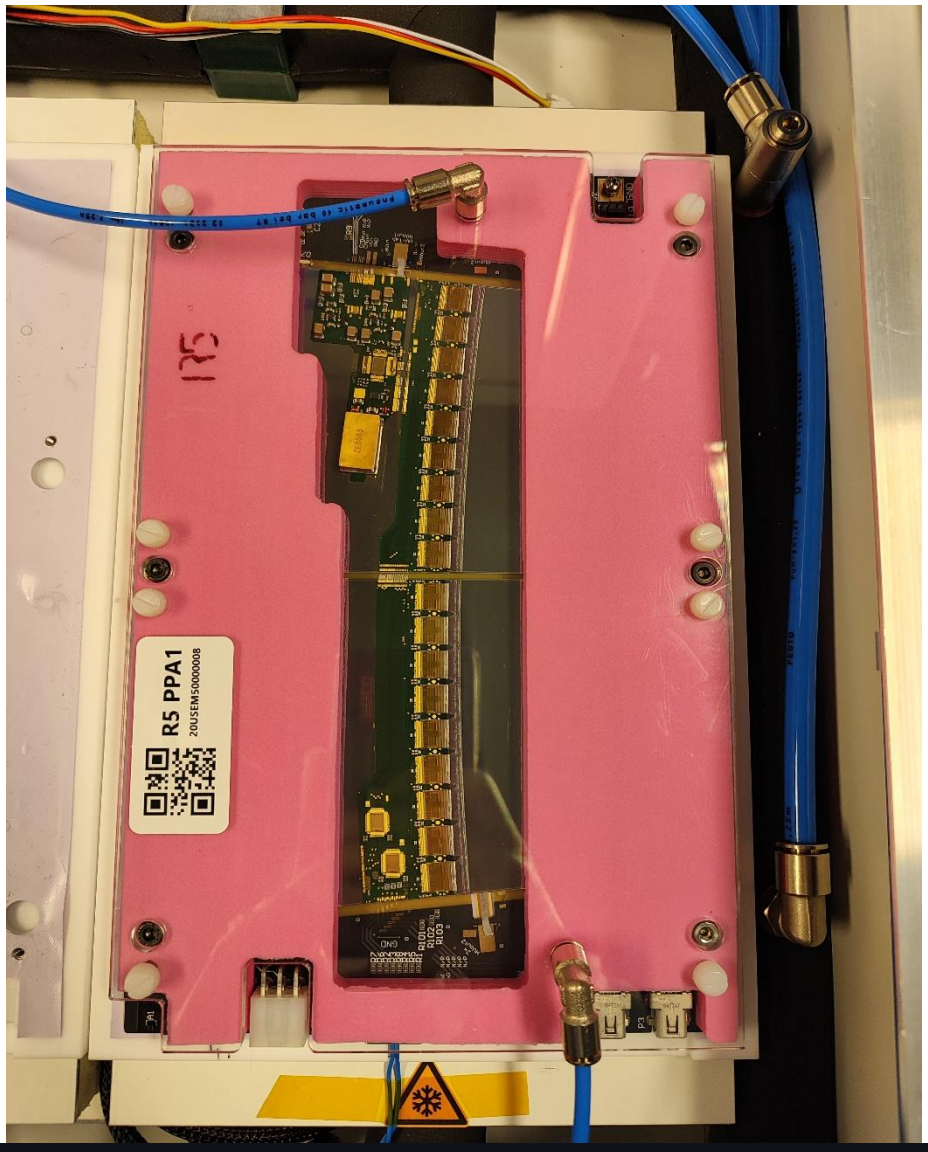

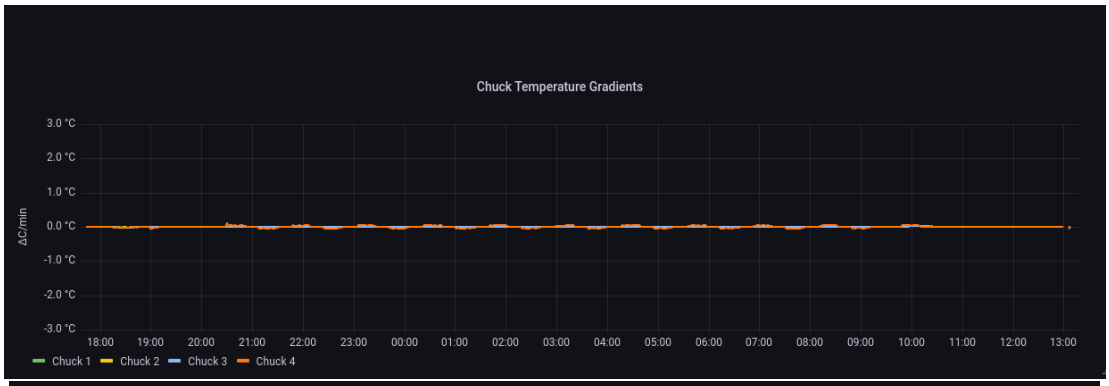
Chuck Temperature Gradients
ΔC/min
3.0 °C
2.0 °C
1.0 °C
0.0 °C
-1.0 °C
-2.0 °C
-3.0 °C
18:00 19:00 20:00 21:00 22:00 23:00 00:00 01:00 02:00 03:00 04:00 05:00 06:00 07:00 08:00 09:00 10:00 11:00 12:00 13:00
Chuck 1 Chuck 2 Chuck 3 Chuck 4


Chiller
Temperature
20.0 °C
0.0 °C
-20.0 °C
18:00 19:00 20:00 21:00 22:00 23:00 00:00 01:00 02:00 03:00 04:00 05:00 06:00 07:00 08:00 09:00 10:00 11:00 12:00 13:00
Set Temperature Internal Temperature

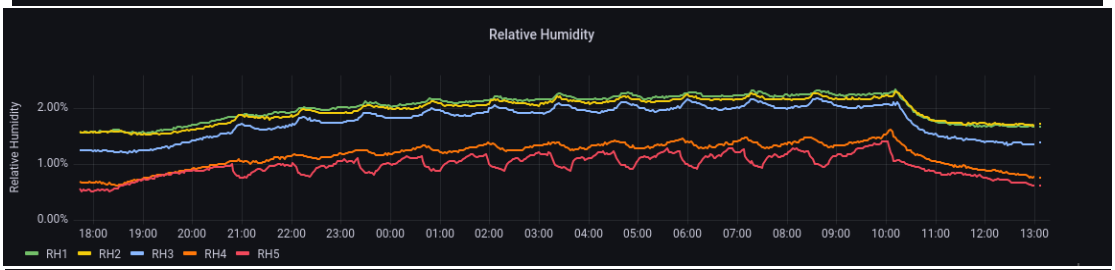
Relative Humidity
Relative Humidity
2.00%
1.00%
0.00%
18:00 19:00 20:00 21:00 22:00 23:00 00:00 01:00 02:00 03:00 04:00 05:00 06:00 07:00 08:00 09:00 10:00 11:00 12:00 13:00
RH1 RH2 RH3 RH4 RH5

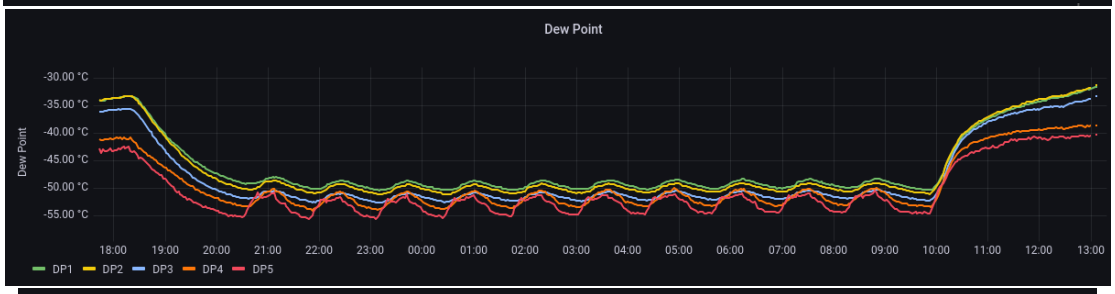
Dew Point
Dew Point
-30.00 °C
-35.00 °C
-40.00 °C
-45.00 °C
-50.00 °C
-55.00 °C
18:00 19:00 20:00 21:00 22:00 23:00 00:00 01:00 02:00 03:00 04:00 05:00 06:00 07:00 08:00 09:00 10:00 11:00 12:00 13:00
DP1 DP2 DP3 DP4 DP5

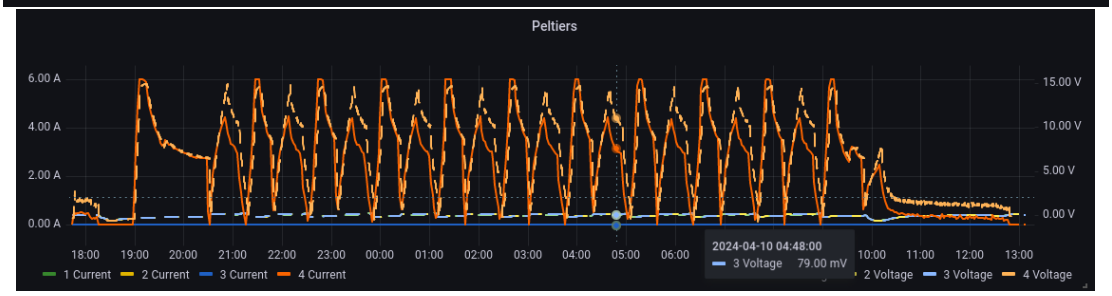
Peltiers
6.00 A
4.00 A
2.00 A
0.00 A
15.00 V
10.00 V
5.00 V
0.00 V
18:00 19:00 20:00 21:00 22:00 23:00 00:00 01:00 02:00 03:00 04:00 05:00 06:00 10:00 11:00 12:00 13:00
2024-04-10 04:48:00
3 Voltage 79.00 mV
1 Current 2 Current 3 Current 4 Current
2 Voltage 3 Voltage 4 Voltage

Figure 22: Test result of the 10 cycle test with an R5 on Chuck 4. Note for that the relative humidity plots, the sensors were not yet connected to the module-specific air outlets, but all just lying freely in the box.

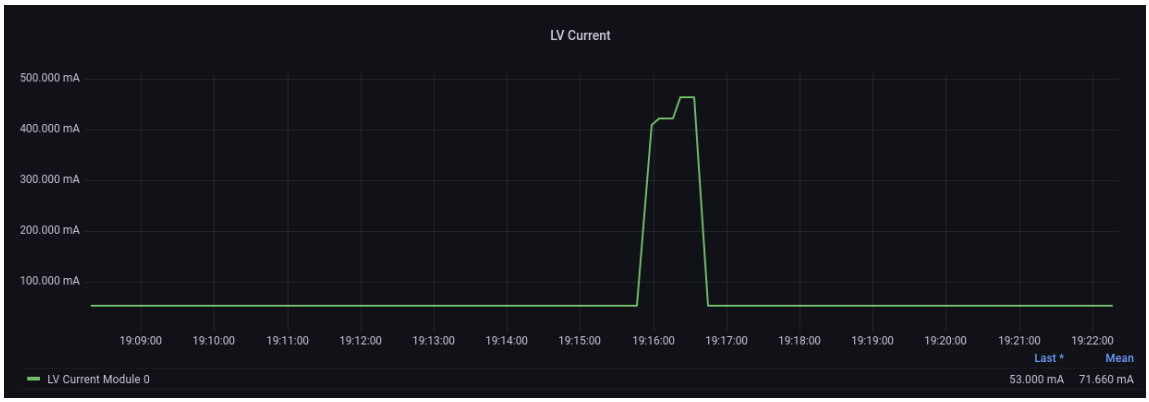

Figure 23: Cold turn-on test

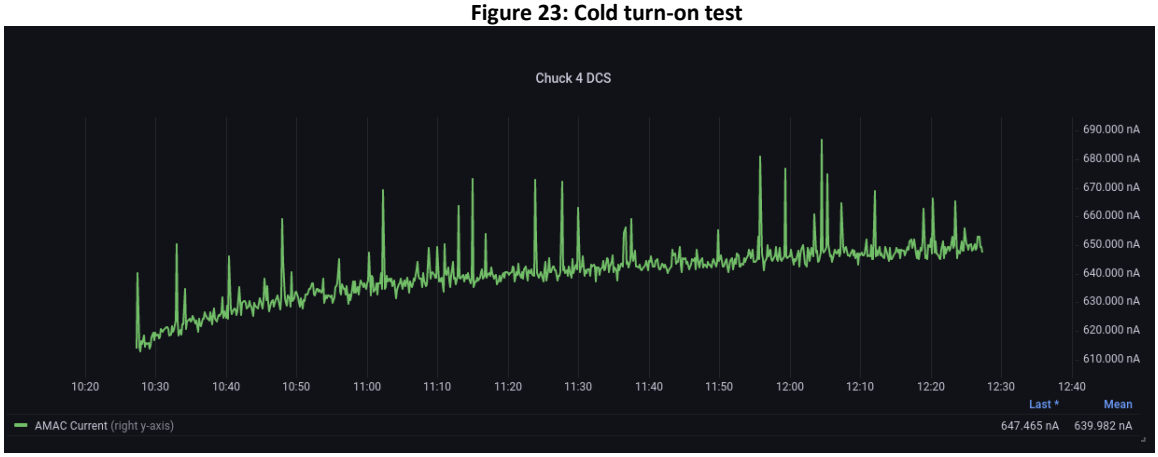

Figure 24: HV Stability test at the end of the cycle. This is an AMACv2, so HVRet was only recorded (with that name) during the HV Stability test. For AMACStar this curve would start at the beginning of the cycle.

Database interaction: Uploaded data

R5 module link: https://itkpd-test.unicorncollege.cz/componentView?code=23b688db5ce5db5ccb5bb78cd72a4082

R5H0 hybrid link: https://itkpd-test.unicorncollege.cz/componentView?code=67cb218ffd644161c6c950fc39385284

- PEDESTRAL_TRIM_TC: https://itkpd-test.unicorncollege.cz/testRunView?id=661ef01a15f2550035682faa
- STROBE_DELAY_TC: https://itkpd-test.unicorncollege.cz/testRunView?id=661ef01a5e538000342bb0b4
- RESPONSE_CURVE_TC: https://itkpd-test.unicorncollege.cz/testRunView?id=661ef01915f2550035682f84
- NO_TC: https://itkpd-test.unicorncollege.cz/testRunView?id=661ef01815f2550035682f6f

R5H1 hybrid link: https://itkpd-test.unicorncollege.cz/componentView?code=ac58b0e733b801f148e2161bb57b6c42

- PEDESTRAL_TRIM_TC: https://itkpd-test.unicorncollege.cz/testRunView?id=661ef1fd15f25500356831f0
- STROBE_DELAY_TC: https://itkpd-test.unicorncollege.cz/testRunView?id=661ef1fb5e538000342bb2ed
- RESPONSE_CURVE_TC: https://itkpd-test.unicorncollege.cz/testRunView?id=661ef1fc15f25500356831ce
- NO_TC: https://itkpd-test.unicorncollege.cz/testRunView?id=661ef1fb5e538000342bb2db